Åbo Akademi
University

Motolani Sakeye

Metal Oxides Prepared through the Nanocasting Approach-Mechanistic Study, Surface Interactions and Applications in Separation

Motolani Sakeye

Education

B.Sc. Chemical Engineering, Obafemi Awolowo University, Ile-Ife, Nigeria.
M.Sc. (Tech) Chemical Engineering, Åbo Akademi University, Finland.

Research Interests

Porous materials synthesis, surface chemistry & surface interactions of porous materials, separation, catalysis, energy storage & conversion.

Metal Oxides Prepared through the Nanocasting Approach-Mechanistic Study, Surface Interactions and Applications in Separation

Motolani Sakeye

Laboratory of Physical Chemistry
Faculty of Science and Engineering
Åbo Akademi University
Åbo, Finland 2016

Supervised by:

Docent Jan-Henrik Smått
Laboratory of Physical Chemistry
Åbo Akademi University
Finland

Prof. Jouko Peltonen
Laboratory of Physical Chemistry
Åbo Akademi University
Finland

Reviewed by:

Professor Dr. An-Hui Lu
School of Chemical Engineering
Dalian University of Technology,
P. R. China

and

Dr. Rachel A. Caruso
Associate Professor & Reader
School of Chemistry,
The University of Melbourne,
Australia

Opponent:

Professor Dr. An-Hui Lu
School of Chemical Engineering
Dalian University of Technology,
P. R. China

ISBN 978-952-12-3376-0 (Print)
ISBN 978-952-12-3377-7 (Electronic)
Painosalama Oy – Turku, Finland 2016

“*To whom much is given, much is expected*”

Luke 12:48 (Holy Bible)

CONTENTS

ABSTRACT

Mesoporous metal oxides are nowadays widely used in various technological applications, for instance in catalysis, biomolecular separations and drug delivery. A popular technique used to synthesize mesoporous metal oxides is the nanocasting process. Mesoporous metal oxide replicas are obtained from the impregnation of a porous template with a metal oxide precursor followed by thermal treatment and removal of the template by etching in NaOH or HF solutions. In a similar manner to the traditional casting wherein the product inherits the features of the mold, the metal oxide replicas are supposed to have an inverse structure of the starting porous template. This is however not the case, as broken or deformed particles and other structural defects have all been experienced during nanocasting experiments. Although the nanocasting technique is widely used, not all the processing steps are well understood. Questions over the fidelity of replication and morphology control are yet to be adequately answered. This work therefore attempts to answer some of these questions by elucidating the nanocasting process, pin pointing the crucial steps involved and how to harness this knowledge in making wholesome replicas which are a true replication of the starting templates.

The rich surface chemistry of mesoporous metal oxides is an important reason why they are widely used in applications such as catalysis, biomolecular separation, etc. At times the surface is modified or functionalized with organic species for stability or for a particular application. In this work, nanocast metal oxides (TiO_2, ZrO_2 and SnO_2) and SiO_2 were modified with amino-containing molecules using four different approaches, namely (a) covalent bonding of 3-aminopropyltriethoxysilane (APTES), (b) adsorption of 2-aminoethyl dihydrogen phosphate (AEDP), (c) surface polymerization of aziridine and (d) adsorption of poly(ethylenimine) (PEI) through electrostatic interactions. Afterwards, the hydrolytic stability of each functionalization was investigated at pH 2 and 10 by zeta potential measurements. The modifications were successful except for the AEDP approach which was unable to produce efficient amino-modification on any of the metal oxides used. The APTES, aziridine and PEI amino-modifications were fairly stable at pH 10 for all the metal oxides tested while only AZ and PEI modified-SnO_2 were stable at pH 2 after 40 h. Furthermore, the functionalized metal oxides (SiO_2, Mn_2O_3, ZrO_2 and SnO_2) were packed into columns for capillary liquid chromatography (CLC) and capillary electrochromatography (CEC). Among the functionalized metal oxides, aziridine-functionalized SiO_2, (SiO_2-AZ) showed good chemical stability, and was the most useful packing material in both CLC and CEC.

Lastly, nanocast metal oxides were synthesized for phosphopeptide enrichment which is a technique used to enrich phosphorylated proteins in biological samples prior to mass spectrometry analysis. By using the nanocasting technique to prepare the metal oxides, the surface area was controlled within a range of 42-75 m^2/g thereby enabling an objective comparison of the metal oxides. The binding characteristics of these metal oxides were compared by using samples with different levels of complexity such as synthetic peptides and cell lysates. The results show that nanocast TiO_2, ZrO_2, Fe_2O_3 and In_2O_3 have comparable binding characteristics. Furthermore, In_2O_3 which is a novel material in phosphopeptide enrichment applications performed comparably with standard TiO_2 which is the benchmark for such phosphopeptide enrichment procedures. The performance of the metal oxides was explained by ranking the metal oxides according to their isoelectric points and acidity.

Overall, the clarification of the nanocasting process provided in this work will aid the synthesis of metal oxides with true fidelity of replication. Also, the different applications of the metal oxides based on their surface interactions and binding characteristics show the versatility of metal oxide materials. Some of these results can form the basis from which further applications and protocols can be developed.

SVENSK SAMMANFATTNING

I dagens läge är mesoporösa metalloxider (med en porstorlek 2–50 nm) mycket viktiga inom ett flertal teknologiska och industriella användningsområden. De används bl.a. som adsorbenter, katalysmaterial, och för separering av biomolekyler. Mesoporösa metalloxider har en stor ytarea, en smal porstorleksfördelning, samt ett högt yta-per-volym-förhållande, vilka alla är fördelaktiga egenskaper inom just dessa användningsområden. Till exempel ger den stora ytarean samt den smala porstorleksfördelningen möjlighet till adsorption och separering av ämnen, medan porutrymmena kan fungera som ett redskap för att transportera mediciner till infekterade celler.

Nanocasting (*sv.* nano-gjutning) är en av de metoder som kan användas för att tillverka mesoporösa metalloxider. Metoden är lik traditionell gjutning där ett råmaterial (t.ex. lera eller betong) hälls i en gjutform som används för att ge den stelnade leran eller betongen en önskad form. Det producerade materialet behåller således samma struktur som gjutformen efter att formen tagits bort. Man kan alltså jämföra nanocastingprocessen med traditionell gjutning, men i det här fallet sker alltså replikeringen på nanoskalan i stället för på makroskopisk nivå. I processen används porösa kiseloxidmaterial (såsom mesoporösa SBA-15 partiklar) som gjutformar, d.v.s. ”templat”. Framställningen av metalloxider genom nanocastingmetoden innebär att det porösa templatet först impregneras med en metallsaltlösning av den önskade oxiden, vilket åtföljs av en värmebehandling (”kalcinering”), och slutligen avlägsnas kiseloxidtemplatet genom etsning i en alkalisk lösning. Den replikerade metalloxiden erhåller således en liknande porös struktur som templatet.

Avhandlingen är indelad i fyra sammankopplade delar, där den första delen belyser själva nanocastingprocessen. Den följer metallsaltets väg från impregneringsskedet till övergången till metalloxid. Den andra delen behandlar ytmodifieringen av de nanoreplikerade metalloxiderna vilket är grundläggande för tillämpningarna av dessa material. De sista två delarna gäller användningen av materialen inom kromatografi samt fosfopeptidanrikning.

Denna studie av nanocastingprocessen ger en klarare bild av de olika processeringsstegen, vilket leder till att porösa metalloxider av hög kvalitet lättare kan framställas. Med fokus på ytväxelverkningar samt bindningskaraktären medför karakteriseringen av de mesoporösa metalloxiderna också en grundläggande förståelse som möjliggör utvecklingen av nya typer av tillämpningsområden för dessa material.

LIST OF ABBREVIATIONS AND SYMBOLS

BET	Braunner-Emmett-Teller theory for surface area determination
BJH	Barrett-Joyner-Halenda method for deriving pore sizes
d, D	Pore diameter and particle diameter
DFT	Density functional theory
DSC	Differential scanning calorimetry
EDS	Energy dispersive spectroscopy
FTIR	Fourier transform infrared spectroscopy
IEP	Isolelectric point
In situ	From latin: “typically refers to a method of data collection or manipulation of a sample without exposure to an external environment”
Ex situ	A method of data collection from a sample exposed to an external environment
P/P_0	Relative pressure
SAXS	Small angle x-ray scattering
SBA	Santa Barbara Amorphous
SEM	Scanning electron microscopy
TEM	Transmission electron microscopy
TG/DTA	Thermo-gravimetric/differential thermal analysis
UV-vis	Ultra-violet- Visible light spectroscopy
ζ	Zeta potential
λ	Wavelength

LIST OF PUBLICATIONS

I. **A Detailed Study of the Nanocasting Process by In Situ X-Ray Scattering and Diffraction**
Motolani Sakeye, Sebastian Ziller, Heinz Amenitsch, Mika Lindén, and Jan-Henrik Smått, *Journal of Physical Chemistry C*, 120 (2016) 1854–1862.

II. **Comparison of Different Amino-Functionalization Procedures on a Selection of Metal Oxide Microparticles – Degree of Modification and Hydrolytic Stability**
Motolani Sakeye and Jan-Henrik Smått, *Langmuir*, 28 (2012) 16941-16950.

III. **Polyethylenimine-modified metal oxides for fabrication of packed capillary columns for capillary electrochromatography and capillary liquid chromatography**
Susanne K Wiedmer, Giovanni D'Orazio, Jan-Henrik Smått, Delphine Bourdin, Clara Baños-Pérez, Motolani Sakeye, Maarit Kivilompolo, Matias Kopperi, José Ruiz-Jiménez, Salvatore Fanali, Marja-Liisa Riekkola, *Journal of Chromatography A*, 1218 (2011) 5020-5029.

IV. **A systematic evaluation of nanocast metal oxide microspheres for phosphoproteomics applications**
Alexander Leitner, Motolani Sakeye, Christian Zimmerli, Jan-Henrik Smått
Manuscript submitted.

SUPPORTING PAPERS

Removal of Intrawall Pores in SBA-15 by Selective Modification
Nina Reichhardt, Tomas Kjellman, Motolani Sakeye, Filip Paulsen, Jan-Henrik Smått, Mika Lindén, Viveka Alfredsson, *Chemistry of Materials* 15 (2011) 3400-3403.

Phospholipids covalently attached to silica particles as stationary phase in nano-liquid chromatography
Clara-Eugenia Baños, Susanne K Wiedmer, Jan-Henrik Smått, Motolani Sakeye, Jana Lokajová, Marja-Liisa Riekkola, *Journal of Pharmaceutical and Biomedical Analysis* 71 (2012) 1-10.

Independent Fine-Tuning of the Intrawall Porosity and Primary Mesoporosity of SBA-15
Tomas Kjellman, Nina Reichhardt, Motolani Sakeye, Jan-Henrik Smått, Mika Lindén, Viveka Alfredsson, *Chemistry of Materials* 25 (2013) 1989-1997.

CONTRIBUTION OF THE AUTHOR

The author is responsible for all the experimental work in the thesis except:

TEM images in Paper I were recorded by Dr. Sebastian Ziller.

In-situ SAXS measurements and data analysis were done at the Elettra synchrotron facilities in Trieste, Italy by Dr. Jan-Henrik Smått and Prof. Mika Lindén in collaboration with Dr. Heinz Amenitsch.

Analysis of XRD and SAXS measurements in Paper I was done in collaboration with Dr. Jan-Henrik Smått, Prof. Mika Lindén and Dr. Heinz Amenitsch.

SEM images in Paper II recorded by MSc. Linus Silvander.

Chromatography experiments in Paper III were done by Dr. Susanne Wiedmer's group in the University of Helsinki.

SEM images in Paper III were recorded by Dr. Mikael Järn.

Aziridine synthesis in Papers II and III were done by MSc. Alain Duchanoy.

All XRD measurements were made by Dr. Jan-Henrik Smått.

Phosphopeptide enrichment tests and data analysis in Paper IV were done in collaboration with Dr. Alexander Leitner.

1. INTRODUCTION

Materials such as wood, clay and hides are natural materials with varying degrees of porosity that man has used for shelter, clothing and as raw materials in pre-historic times. Man-made porous materials such as cement and mortar were later produced for stronger structures as knowledge advanced. Advancement in industrial processes in the 19th and 20th centuries further accelerated the development of highly porous solids such as zeolites, activated carbon, silica gels and aluminas. For example, early synthesis for the preparation of porous metal oxides involved thermal decomposition of a metal salt or calcination of hydroxide or hydrous oxide obtained by a precipitation procedure [1]. The progress in such procedures led to the production of aerogels and subsequently to the development of the sol-gel process.

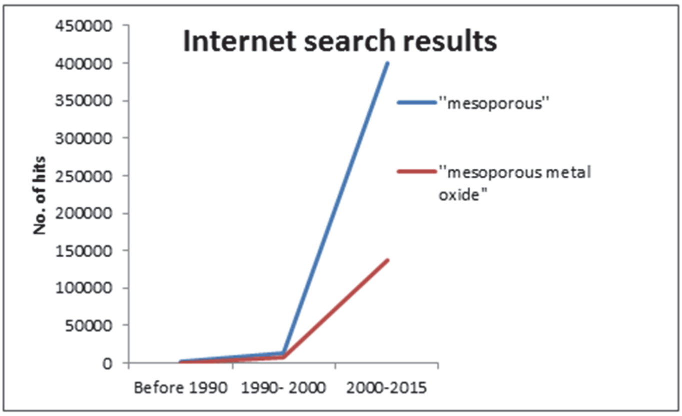

The discovery of ordered mesoporous materials like the M41S group of materials in the 1990s took the interest in porous materials to a higher notch. Internet search with *Google scholar* produced 443,000 hits using the words “mesoporous materials” and 136,000 hits when “mesoporous metal oxides” was typed in. The majority of the articles found discussed order, porosity, syntheses and applications of these materials. The huge number of articles on porous materials and their applications show that the field of porous materials research is rapidly growing with many branches and numerous opportunities opening up [1-3].

Metal oxide materials with mesoporous structures (i.e. pore width between 2–50 nm [4]) may be regarded as nanomaterials because the pores are on the nanoscale. According to the IUPAC definition [5], porous materials are divided into three classes: microporous (<2 nm), mesoporous (2–50 nm) and macroporous (>50 nm). They have a wide range of applications including catalysis [6], adsorption and separation [7, 8], sensors [9, 10], storage devices [11], drug delivery and imaging [12, 13] to mention a few. Besides the use of mesoporous metal oxides in new applications or in novel devices, they are becoming alternatives to some traditional materials as they are less expensive, more efficient, and easier to produce [14-16]. Mesoporous materials have large surface area with narrow pore size distribution and high surface-to-volume ratios. They also have a high surface energy, increased grain boundaries and excellent optical properties. For example, the semi-conducting property of mesoporous titanium oxide is combined with its large surface area to harvest energy from sunlight in dye-sensitized solar cells [17]. The high surface-to-volume ratio and high surface energy also lead to significantly lower melting points and phase transition temperatures compared to bulk materials. The surface energy becomes dominant while cohesive energy and vacancy formation reduces. The lower melting point makes working with or processing of porous materials easier compared to the bulk materials [18]. The increased surface energy coming from more interface alongside more grain boundaries are also reasons for electronic and magnetic properties such as ferromagnetism (as observed in transition metal doped ZnO and TiO_2), and superparamagnetism in nanoparticles used in some imaging techniques [19] and spintronics [20].

The large surface areas of mesoporous materials are highly beneficial for catalyzing reactions. When mesoporous metal oxides are used as support materials, the large surface area enables a high dispersion of the catalytic agents deposited on the surface. Thus highly dispersed catalysts are obtained. This is highly desirable in the catalysis community. The large surface areas and narrow pore size distribution are also favorable for adsorption and separation as the high surface-to-volume ratio resulting from the porosity increases the rate of diffusion. Similarly, as a result of large surface area and increased porosity, the pores and pore walls of mesoporous materials have become a very useful medium in drug delivery. The pore surface and pore walls serve as a medium through which drug compounds can be released to diseased cells [21].

Furthermore, mesoporous metal oxide materials are thermally stable [22] and durable [14] compared to mesoporous silica or polymers. Some polymers tend to deform when the temperature gets as high as 400 °C thus affecting their performance while mesoporous silica sinters at elevated temperatures (about 600 °C). However, mesoporous metal oxides are able to cope at such temperatures [22] and possess mechanical strength (able to withstand high pressure operation and packing in chromatography for example). The thermal stability allows processes to be carried out at high temperatures, and in some applications such as chromatography the durability of porous metal oxides provides a stable platform at wide pH ranges. For instance, at pH values below 2 or above 10 porous silica begins to dissolve in aqueous media while transition metal oxides in general are able to withstand the whole pH range. These are some of the properties and applications of metal oxide nanoparticles which have made them become so invaluable to modern technological endeavors. For instance, metal oxides such as zirconia (ZrO_2) and titania (TiO_2) are used in chromatographic columns as alternative stationary phase to silica. This is because these metal oxides are able to operate at high temperatures and over a wide pH range [23].

The developments highlighted above clearly show the need for fast and inexpensive methods for synthesizing nanoporous materials. Even though the development of porous materials is not a novel idea, the challenge over the last couple of decades has been to control the structural, compositional and morphological features such as pore size distribution, pore volume and surface area which are critical and specific to different applications. There are many pathways by which porous solids are created, the choice of a pathway is largely dependent on the kind of material desired. One common description of pathways divides porous materials synthesis into two basic ways depicting the approach into producing the desired materials. These descriptions are ‘top-down’ approaches and ‘bottom-up’ approaches. Top-down approaches start from a large and already existing component and use various sophisticated tools and techniques to produce smaller pieces with desired properties. A bulk material is restructured and scaled to suit the desired purpose by techniques such as milling, sieving or lithography. The bottom-up approach on the other hand begins with the synthesis of desired materials from atomic and molecular pieces. This approach is based on chemical and physical principles like molecular self-assembly, nucleation and growth, polymerization reactions and sol-gel reactions. Figure 1 shows a summary of the two approaches and their features. The bottom-up approach is preferred as structural order and morphology can be easily controlled with this approach. This approach is also less energy consuming and more cost effective.

An example of a bottom-up technique is nanocasting. This technique is widely used in the synthesis of nanoporous metal oxide materials [3]. It consists of impregnation of hard templates with metal salts or alkoxides and thermal treatment known as calcination, after which the templates are sacrificed and the metal oxides are obtained

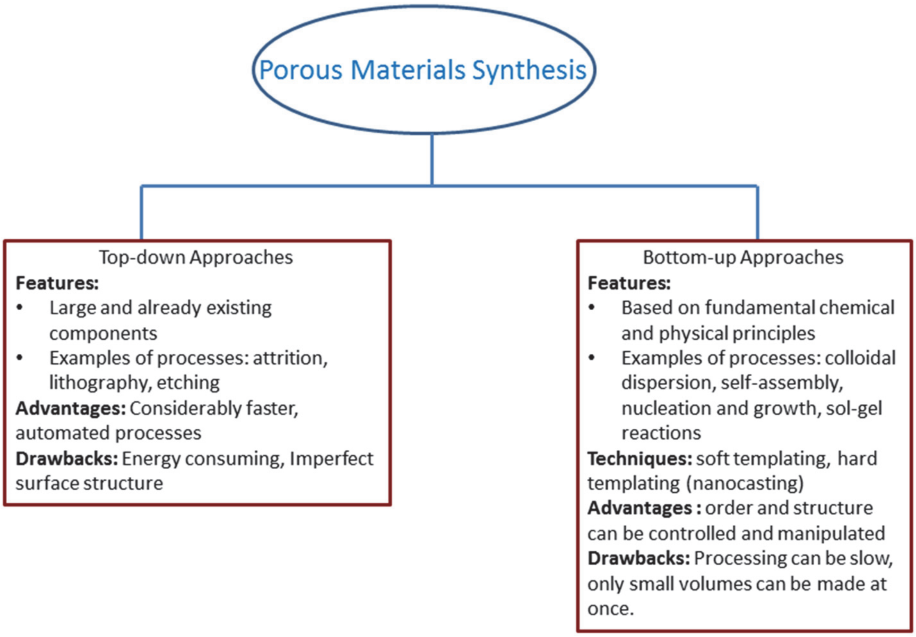

Figure 1: Alternative approaches to porous materials synthesis.

The surface chemistry of mesoporous metal oxides is also important as this is the medium by which metal oxides interact with other molecules and species. For example, the hydroxyl groups and the metal-oxygen bonds on the surface of metal oxides interact with other functional groups such as carboxylic acids or amino groups. These kinds of interactions serve as the basis for most of the interesting applications of metal oxides. Chemical properties such as surface acidity and basicity can be related to the hydro-oxo bridges, oxygen atoms and the metal cations and anions on the surface of metal oxides. These may act as Lewis or BrØnsted acids and bases [14, 15]. The applications of mesoporous metal oxides in molecular separation are based on the surface interactions. For example, the binding at low pH and elution at high pH of phosphopeptides is based on such interactions. Surface modification and functionalization is another example of interactions of the metal oxide surface. Various organic compounds such as phosphonates, silanes and amines may be used as metal oxide modifiers. For instance, 3-(aminopropyl)-triethoxysilane was used in modifying the silica surface before the covalent binding of glutaraldehyde molecule [24]. Modification of a metal oxide surface by a phosphonate can likewise be used to create M-O-P bonds. Titania surfaces modified with phosphonic acid are very stable towards hydrolysis [7]. Hydrolytic stability is an essential consideration in the application of metal oxides. The bond formed through surface modification should be able to withstand hydrolysis in either basic or acidic conditions over a particular period of time. After the surface is modified with an organic molecule which serves as a linker, a functional group may be added to give the material its functionality [7, 24]. The reaction of the functional group with the modified metal oxide surface is also based on the surface chemistry of the metal oxides. The functional groups are coupled via surface interactions such as surface polymerization or adsorption.

1.1. Outline of the thesis

The focus of this doctoral thesis is divided into four interlinked parts. The first part is the elucidation of the process of nanocasting in the synthesis of metal oxides. The second part is on interactions on the surface of the metal oxide materials, while the third and fourth parts show the applications of nanocast metal oxides in different separation processes. Figure 2 is a schematic representation of the thesis outline and how the parts are interlinked.

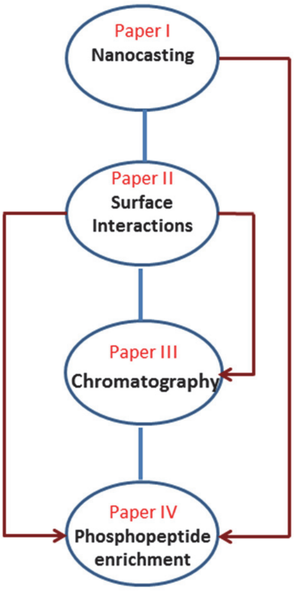

Figure 2: Schematic representation of the thesis outline.

Even though the process of nanocasting has continued to draw a lot of attention since its emergence as a popular technique for synthesizing porous materials in the early 2000s, not all the steps involved in producing wholesome and true replicas has been fully understood or explained. Products of the nanocasting technique are supposed to be negative replicas of their template; however this has not always been the case. The fidelity of the replicas is sometimes questionable as replicas do not depict exact morphological properties as the starting template [25]. Many suggestions have been proffered by different researchers on how to overcome problems such as pore filling, transformation to the oxide and replica fidelity which affect the quality of the replicas. The first article in this thesis (Paper I) looks at the fundamental principles guiding the nanocasting technique. It traces the path of the metal oxide precursor from the impregnation stage till its conversion to the metal oxide. Using *in situ* techniques such as SAXS, XRD, TGA, and DSC complemented with *ex situ* TEM and nitrogen physisorption, it expounds the mechanism of the nanocasting process by pin-pointing the events at each stage of the process in a continuous manner.

The second part of the thesis is based on the surface chemistry and interactions of the metal oxides which were replicated using the fundamental principles garnered in Paper I. In Paper II, four different metal oxides were functionalized with amino groups using four different approaches. The approaches were based on different interactions of the amino-containing molecules with the hydroxyl groups on the metal oxide surface. Functionalization via the different interactions and the stability of these functional groups on the surface of the metal oxides were discussed in the paper. Paper III is on the application of nanocast metal oxides in chromatography. The performance of the functionalized metal oxides as packing material was compared with that of silica which is the traditional material used in such applications. In Paper IV, different metal oxides were synthesized using the nanocasting technique which enabled materials with similar morphological and textural properties to be obtained. These nanocast metal oxides were then used for enrichment of phosphopeptide. The surface chemistry of the metal oxides and the binding characteristics which enabled the identification and quantification of the phosphorylation sites were considered in the paper.

2. NANOCASTING

The nanocasting technique has been described by Lu et al. as "a versatile strategy for creating nanoporous materials" [3], because different shapes, sizes and morphological structures can be synthesized with the technique. Using the nanocasting technique porous particles, films and monoliths, have been synthesized [2, 26, 27]. The technique enables the control of the size and shape of the synthesized materials down to the nanometer length scale by using suitable templates and processing conditions.

Nanocasting can simply be regarded as 'nano-casting', i.e. casting on the nanometer length scale [28]. Casting as a technology has been used since pre-historic times; tools, jewelries and artefacts were casted to suit various purposes. The nanocasting process is quite similar to traditional casting. A mold is filled with liquid or fluid mixture followed by a process of conversion into the desired product and concluded by removing the mold or template. A typical nanocasting process starts with the impregnation of a template by a precursor, followed by the conversion to the product and then the removal of the template in the final stage.

It should be pointed out at this juncture that there are two different ways of synthesizing mesoporous materials namely soft templating and hard templating, both are sometimes erroneously classified as nanocasting. The two ways are however different. In soft templating, the shape and size of the pores are controlled by the use of structure directing agents which control the surface tension or interface between liquids during the synthesis and thus determine the porosity of the material synthesized. In hard templating, a solid porous material is used to control the formation and development of the pores.

2.1. Nanocasting scheme

Synthesis of mesoporous solids via nanocasting entails impregnation (or infiltration) of the porous templates with a precursor, and then drying which is followed by a thermal treatment procedure known as calcination before the template is etched. A typical nanocasting scheme is shown in Figure 3.

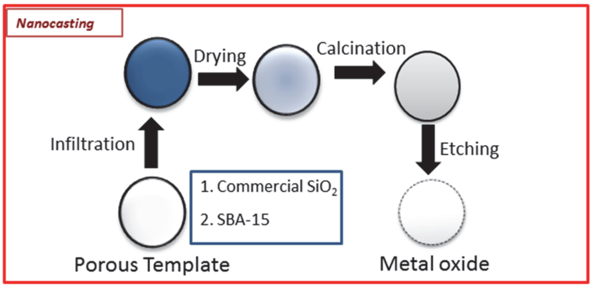

Figure 3: Nanocasting scheme for metal oxide synthesis.

2.1.1. Templates

The nanocasting process starts with choosing a suitable template for the process. A good template should have the morphology desired in the replica product with interconnected pore structure and should be able to withstand the high temperature occurring during the nanocasting process. The template materials should also be strong in order to avoid structural collapse during synthesis but should be easily removable after the process. Powders, films and monoliths of porous silica and carbon have all been used as templating materials [2, 3, 29]. The product of nanocasting depends on the porous matrix used in the synthesis; therefore selecting a suitable matrix which will give the desired morphology and structural characteristics is crucial. The porous matrix or template functions as a rigid skeleton providing support, stability and preventing the collapse of the pore system of the product during post-synthesis handling. Materials with different pore architectures have been used as templates in nanocasting. For example, gold nanorods were synthesized using nanotubules from alumina membranes [30, 31]. Inverse opals are another example and are prepared from ordered arrays of uniformly sized polymer spheres [32, 33]. Other examples of materials used as template are mesoporous carbon, silica and polymers. Mesoporous silica is preferred as a hard template because the rigid framework of the silicate gives structural stability during thermal treatment. The stable replicas are thus prevented from collapse when the template is later removed. Silica is also able to withstand local strain caused by crystallization of precursors, and thus exclude the risk of phase separation during the formation of solid. Furthermore, the wetting behavior of mesoporous silica provides a favorable interaction between the precursor or the polar solvent, and the pore walls of the template material. These factors subsequently ensure that a coherent material is formed. Another reason for choosing silica is that the silica structure is easily controlled and removed in the final stage of the synthesis. Some silica templates used in nanocasting include silica monoliths [34], MCM-41[35], SBA-15 [2, 36-38] KIT-6 [35, 38], vinyl-silica [39], FDU-12 [38], etc. In this work, the silica materials LiChroprep Si 60 (5-20 µm) obtained from Merck; M.S. Gel Sil (EP-DF-5-120 Å) from Shiseido; Daisogel (SP-120-10P) and (SP-300-10P) from Daiso and SBA-15 were used as templates.

Mesoporous SBA-15

SBA-15 is highly ordered mesoporous silica which is made up of two-dimensional hexagonal arrays of interconnected channels [40]. The morphology and textural properties are highly tunable and can be easily controlled as it is synthesized under hydrothermal conditions from sol-gel processing. Typical morphologies such as fiber-like, rope-like, doughnut-like and sphere-like have all been successfully synthesized [40-42]. Generally, SBA-15 materials have pore sizes between 5 -10 nm (or even 15 nm), with typical BET surface areas about 900 m^2/g and a pore volume about 1.00 cm^3/g. The wall thickness varies between 3.1 and 5.3 nm [43], the relatively thick pore walls add mechanical stability to the material. It should be noted that the textural properties of

SBA-15 can vary according to the synthesis conditions such as hydrothermal treatment and calcination temperature [43, 44].

A common pathway is dissolution of a surfactant non-ionic triblock co-polymer which acts as a structure directing agent in an acidic aqueous solution. The silicate precursor (tetraethoxysilane [TEOS]) is then added. The structure directing agent is made of three blocks containing two polyethylene oxide (PEO) blocks and one polypropylene oxide (PPO) block. The PPO block is less polar and more hydrophobic than the PEO blocks. Through self-assembly the polymer flocs are arranged into threadlike micelles and through a combination of electrostatic and hydrogen bonding interactions, the silica becomes mesoscopically ordered. The SBA-15 material is well-known for its characteristic micropores, which link the pore channels through the pore walls. This microporosity results from interactions between PEO chains of micelles within a hydration sphere of the PEO. The mesopores and a fair fraction of the micropores in the wall, leads to a dual pore system of large uniform ordered mesopores interconnected by disordered micropores [45-47]. This bimodal feature of SBA-15 is exploited in nanocasting [48]. The next part of the synthesis is the hydrothermal treatment which can be used to control the microporosity, mesopore size and wall thickness. The hydrothermal treatment also induces the complete condensation, solidification and the structural organization leading to the 2D hexagonal structure of SBA-15. The material is calcined or extracted in the final stage of the synthesis and the SBA-15 is obtained. TEM image of SBA-15 showing its array of cylindrical pores and a schematic image of the hexagonal pore structure are depicted in Figure 4.

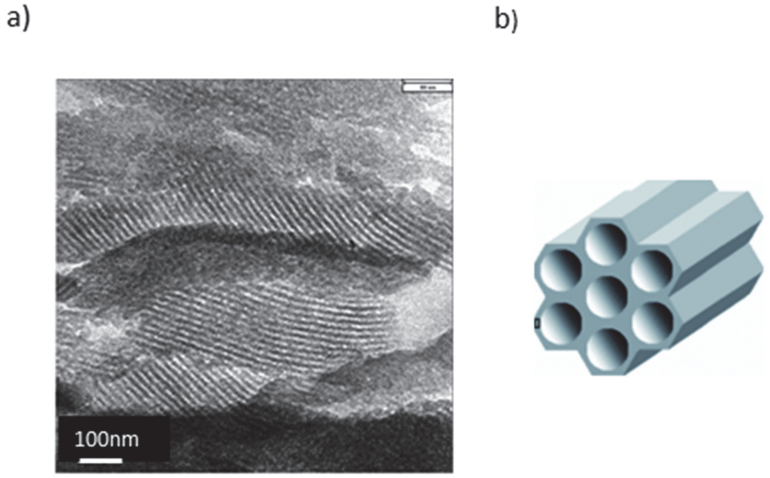

Figure 4: **a)** TEM image of SBA -15 **b)** Schematic representation of SBA-15 matrix [49]. The perpendicular lines seen are the pore channels the hexagonal shape of which is schematically drawn in **b)**.

2.1.2. Infiltration

The first step in the nanocasting routine is the infiltration of the porous matrix of the template with a precursor. The precursor is usually a metal salt or alkoxide (e.g. titanium isopropoxide) of the desired metal oxide. The aim of the infiltration process is to load the precursor into the pores of the templating matrix. The filling of the pores is quite crucial in nanocasting as the success or failure of this stage plays a big role in the structural fidelity of the product. The migration of the precursor into the pores of the templating matrix is affected by interactions such as hydrogen bonding and co-ordination of metal ions by silanol groups, coulombic interactions with oxygen in the pore walls and/or Van der Waals forces [28, 50]. In order to improve the interactions, procedures such as microwave digestion and surface functionalization can be carried out before the infiltration procedures.

2.1.3. Impregnation methods

There are various methods of impregnating the pores of the templating matrix and the nomenclature of such may vary. The most common ones are listed below and schematically depicted in Figure 5.

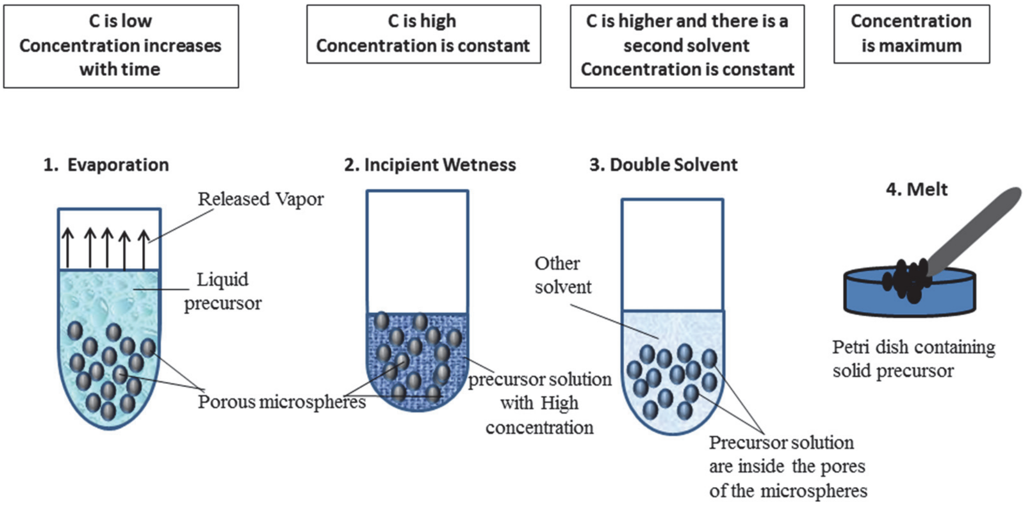

Figure 5: Schematic presentation of the impregnation methods.

a) Evaporation method: The evaporation method is straightforward and widely used [3, 36, 51]. This method is also sometimes described as the wet impregnation method [28]. The precursor is dissolved in a volatile liquid (usually ethanol) and then mixed with the silica template. It is expected that the precursor solution is sucked into the pores by capillary forces while the concentration gradually increases during solvent evaporation.

Solvents used for this method usually have high dissolving ability and weak interaction with the template surface.

b) Incipient wetness method: This impregnation method is based on a prior knowledge of the pore volume of the silica template. The pore volume is pre-determined by nitrogen sorption, and the exact volume of the pores is filled with the precursor solution. By using the exact volume of the template, all the precursor is sucked into the pores of the template thereby leaving little or no precursor material on the outside of the pores [28].

c) Double-solvent method: In this method, two solvents are used as the name implies. The silica template is suspended in a volatile liquid which is immiscible with water, for example dry hexane; while a solution of the precursor in water is then mixed with the silica-hexane suspension. The porous silica template being hydrophilic absorbs the precursor solution while the hexane being hydrophobic forces the precursor solution into the silica pores. This method has also been used extensively to prepare In_2O_3, NiO, Cr_2O_3, and Co_3O_4 among others [37, 38].

d) Melt-infiltration: The melt-infiltration method is also known as the solid-state grinding route [52]. The method introduces the precursor into the silica mesopores of the template by grinding a mixed powder of the precursor and the silica template. The precursor melts as a result of heating and the liquid melt is sucked into the pores of the template. The advantage of this method is that it is solvent-free and therefore more environmentally friendly compared to other methods [53]. Secondly, smaller number of impregnation cycles is required compared to the other methods.

The advantages and drawbacks of each method are listed below.

Impregnation method	Advantage	Drawback
Evaporation	Straightforward and easy to follow	Slow evaporation More solvent required, difficult to control crystallization outside the pores
Incipient wetness	Unwanted extra solvent is avoided	Many cycles of impregnation required
Double-solvent	Quicker pore loading, precursor stays inside the pores, precursor loss is avoided	Handling of two solvents can be complicated, many impregnation cycles are required
Melt-infiltration	Solvent free, higher concentration of precursor, less impregnation cycles	Only precursors with low melting point can be used

Other methods such as chemical vapor deposition (CVD) or physical vapor deposition may also be used [3].

2.1.4. Factors affecting Initial pore loading

A high degree of precursor loading is required for a successful nanocasting process. Capillary force, wettability of the template, mobility of precursor ions and the nature of the solvent are all significant in the filling of the pores of the template. Listed below are some critical issues influencing the precursor loading.

a) Template wetting: The wetting of the template is important. This is because the surface wetting affects the mobility of the precursor solution or melt into the pores and inside the pores. When the solution or melt wets the template, i.e. if the work of adhesion is greater than the work of cohesion, the penetration into the pores is energetically favored. The high pore filling degree eventually leads to a good replication. On the other hand, if the wetting is poor, the mobility of the precursor into the template is slower which may lead to aggregation of the precursor ions at different spots either inside the pores, along the pore walls or outside the pores. Such precursor aggregation may eventually hinder the replication process leading to disordered nanowires or nanoparticles as a result of too weak contact between the precursor and the template [54]. Pre-wetting the silica template with hydrophobic solvent as in the case of double solvent impregnation technique improves the penetration of the precursor inside the pores. There is a slight surface modification of the SBA-15 by a hydrophobic solvent. The addition of an alkane (e.g. n-hexane) causes an increase in the germinal and hydrogen-bonded silanol groups on the silica surface thereby increasing its hydrophobicity [55]. The hydrophobicity in turn hinders the hydrophilic solution of the precursors from moving out from the pores.

In order to load more of the precursor into the pores, the capillary force and the precursor-template ('host-guest') interaction can be improved. Better suction into the pores as a result of improved capillarity will lead to more capillary condensation inside the pores. Similarly, an accurate control of the interaction between the hard host (silica template) and the guest (precursor) or the molecules themselves will also facilitate a host-guest assembly process [50]. Silanol groups located on the pore walls of the template attract guest molecules which participate in the formation of hydrogen bonds and interaction with other electronegative atoms of the precursors. Thus the interaction between the template and the precursor improves significantly when more silanols are retained on the pore walls of the template. Techniques such as microwave digestion (MWD) and solvent extraction are therefore preferred to calcination during the synthesis of templating materials such as SBA-15[36]. These techniques improve the host-guest interaction as well as the wetting. Functional groups of organosiloxanes for example 3-aminopropyltriethoxysilane (APTES), have high coordination abilities which will bring strong interaction with the pore walls and enhance the adsorption of precursor into the mesopores [56]. It should also be mentioned at this juncture that Liu et al. [57] used vacuum to enhance the capillary force in the infiltration process. The residue of gas in the inner pores was forced outwards leading to a balance in the difference in pressure between the pores and the vacuum chamber. The balance in pressure eventually led to an efficient pore infiltration.

b) Precursors: The ideal precursor should have a high density so that it can fill as much of the pore volume as possible when converted to the oxide, thereby minimizing the impregnation cycles. Secondly, such precursors should have a low melting point and high solubility. Low melting point is required as this enables the precursor to melt properly and move into the pores before decomposition. The mobility of the precursor is very crucial to pore filling. Similarly, precursors with high solubility provide good pore filling. Nitrates have reasonable volume yields (about 10%) and they tend to melt at low temperatures before decomposition which is also at relatively low temperature. Oxalates, citrates and acetates have also been used widely in literature. The precursor anions should also have weak coordination ability as a strong coordination inhibits the transportation of metal ions. Polyacids such as phosphotungstic acid (PTA) and phosphomolybdic acid (PMA) have high volume yields up to 90% and are therefore good precursors but they are very rare [3].

During the drying and evaporation of the solvent, the precursor begins to decompose into the target product. Massive gaseous by-products are released, causing mass loss, volume constriction, and density change in the pores of the precursor. Therefore, the volume of metal oxide formed inside the pores is much less than the volume of the precursor solution used for impregnation. Such volume constriction creates vacancies in the pores after one cycle of impregnation, so the impregnation cycle is usually repeated a few times depending on the solvent, precursor and the pore volume of the template. The template material has to be adequately filled in order for the structure of the template to be successfully replicated otherwise the metal oxide structure will collapse when the template support is removed.

c) Solvents: Solvents are required as a medium for conveying the precursor into the template (except in the melt-infiltration method). The precursor needs to be soluble in the solvent of choice, as this will lead to better precursor filling of the template and hence higher infiltration efficiency. The wetting of the template surface by the solvent is also crucial as has been pointed out earlier, as this will improve the capillary force in the porous template and also affect the migration and aggregation of the precursor inside the template.

Ethanol is the most commonly used solvent because most nitrates and chlorides are soluble in it. Moreover, it interacts and wets silica surface as it also evaporates fast. However, water may also be used if the precursor solvates better in water even though the disadvantage with water is its high boiling point and strong hydration effect which may lead to aggregation or clumping of precursor inside the pores of the template as Zhao and Lu have pointed out [3].

2.2. Transformation to the oxide (drying and calcination)

After the silica template has been adequately loaded or impregnated with the precursor salt solution, the next process is drying and thermal treatment of the composite. Drying is the removal of the solvent from the precursor solution after the impregnation. Drying can be carried at room temperature or at temperatures high enough to evaporate the solvent. The thermal treatment also known as 'calcination' is carried out at elevated temperatures under different atmospheric conditions. Gas atmospheres such as air is used to convert the precursor to the metal oxide, though inert atmospheres such as argon or helium may be used for synthesis of materials sensitive to oxygen and therefore may become oxidized in air, for example Cu metal or carbon. The thermal treatment may be divided into two stages. The first stage is the melting stage during which the precursor becomes mobile as it turns into a liquid or molten form. Alongside melting is the removal of the water of crystallization. The second stage is the decomposition stage, wherein the precursor is converted into the product as the precursor decomposes into the oxide. The melting and decomposition may overlap, as the melting may not be concluded before the decomposition starts. The thermal decomposition and conversion to the oxide takes place inside the pores of the hard templates. Gaseous by-products are released as the oxide is formed. The melting stage is crucial because as the precursor turns into the liquid state, it is sucked into the pores of the template thereby filling the pores. At some point during the melting of the precursor, there is precipitation of nucleation 'seeds' from the melt on some sites inside the pores [3, 25, 52, 58]. The size of the nucleation seeds increase after each impregnation round as the new salt deposition adds to existing seeds rather than forming new ones [37]. A simplified scheme of the transformation to the oxide is shown in Figure 6.

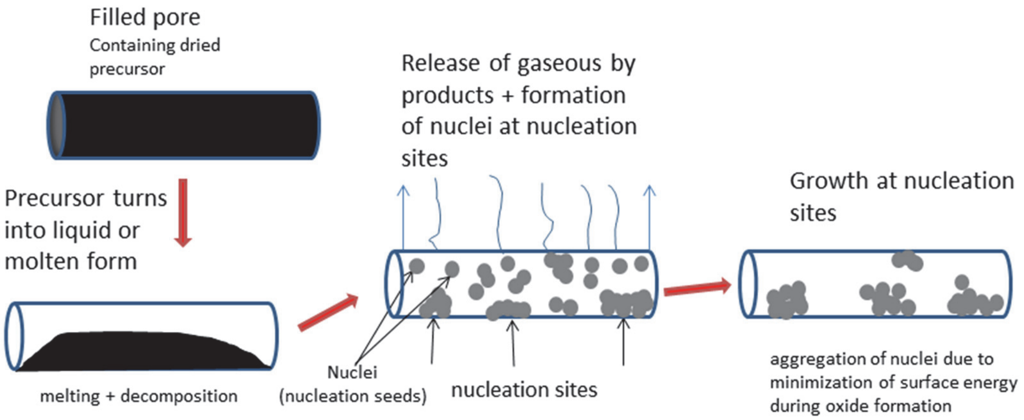

Figure 6: Transformation from the precursor to the oxide.

The growth of the seeds and the release of gaseous by-products have effects on the final products. The melting and decomposition of the precursor is an equilibrium process controlled by the removal of the gaseous by-products of the decomposition. The product of the melting and decomposition can be molten as a result of the precursor melt mixing with the water of crystallization not yet removed, or solid if the reaction proceeds very fast and the water of crystallization dries out. Sun et al. [59] showed that a slow escape of water and gases from the nanocasting sample container makes the nucleation seeds more molten. They subsequently grow larger leading to the formation of large particles. However, if the water of evaporation is allowed to escape, the melt solidifies before it decomposes. The conversion from solidified melt hinders the long distance transport of the ions or species and isolated nanoparticles are formed instead.

The processing temperature is vital in nanocasting. The usual practice is to ramp the heating i.e. to gradually step up the heating relative to time. It is also advisable to choose precursors that decompose at low temperatures, as this enables them to melt completely before decomposing. This in turn allows for better penetration of the precursor into the pores thereby improving the pore filling and enhancing the quality of the replicas. The crystallinity of the oxides can also be controlled with the synthesis temperature [59].

2.3. Template etching

The last stage in the nanocasting scheme is generally known as etching or sometimes leaching. It is the point at which the scaffold or support is sacrificed in order to obtain the metal oxide. The method of removal is dictated by the type of template used. Silica templates are removed with strong alkaline solutions (typically NaOH as shown in Figure 7). HF has also been used although this has to be done with extreme caution as HF is a very toxic chemical. The silica dissolves in an alkaline solution, even though some residual silica remains left. However, if HF is used the amount of silica left is relatively small [3]. Moreover, only certain metal oxides can be etched with HF as it may dissolve the metal oxide alongside the silica.

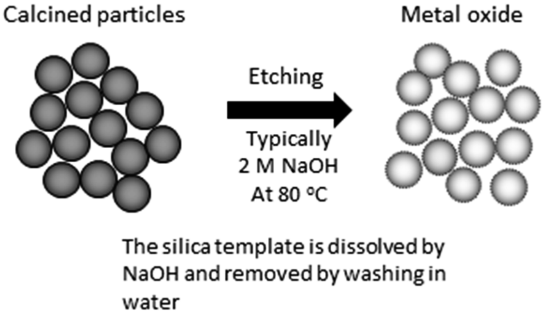

Figure 7: A typical etching procedure.

3. SURFACE MODIFICATION AND FUNCTIONALIZATION

Functionalization of metal oxides is fundamental to some applications of metal oxides and it is one of the reasons for the sustained upward trend of the interest in metal oxide nanomaterials. Applications such as molecular separation and adsorption are based on the coupling of different functional molecules to the surface or pore walls of porous metal oxide materials. Porous materials can be functionalized by incorporating functional species during the synthesis (direct synthesis) or by augmenting the material after the synthesis (post-synthesis) in order to alter the surface chemistry to suit the desired application. Modification and functionalization are often considered as synonyms but they refer to different issues. If a chemical species is coupled to the surface of a metal oxide to serve as a linker for another group or interfere with the surface properties of the oxide, then the species is a linker or modifier and the process is surface modification. Another form of modification occurs when the chemical species interact with the surface groups of the metal oxides. On the other hand, if the molecule is coupled with the aim of performing a particular function, such as adsorption or molecular separation then it is functionalization. The difference therefore lies in the purpose of the coupled chemical species. Some common routes to surface modification and functionalization are shown in Figure 8.

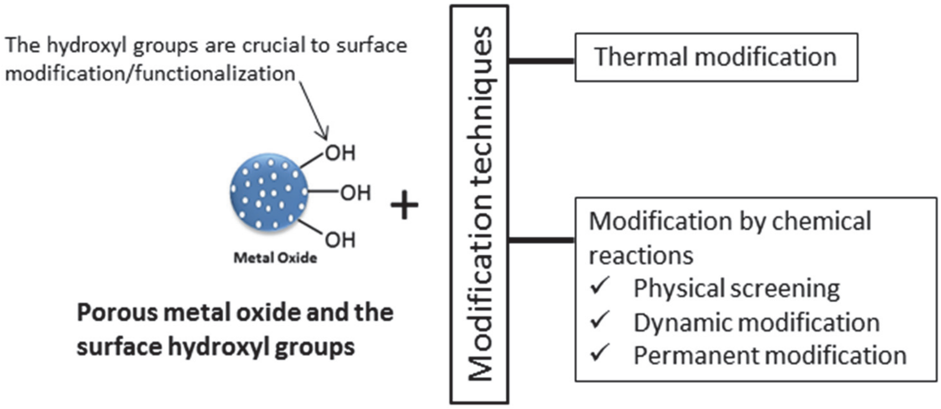

Figure 8: Routes to surface modification/functionalization

3.1. Modification techniques

3.1.1. Thermal modification

Sintering and phase transitions can be considered as a thermal modification technique. Sintering may be described as the process in which fine particles of a material become chemically bonded at a temperature that is sufficient for atomic diffusion [1]. Sintering involves heating the material at elevated temperatures; however this has to be done judiciously as heating to temperature close to the melting point of the solid may lead to a loss of porosity. During the heating of porous solids, removal of adsorbed water and dehydroxylation occurs. If the temperature is sufficient, there can also be a thermal displacement of atoms which may have an effect on the pore system. Sintering can be used to adjust the surface area of mesoporous particles, but this has to be done carefully so that the porosity is not lost nor the crystal phase altered. The thermal displacement of atoms may cause coalescence of grains or rearrangement of the structural order of the atoms. Such rearrangement may lead to a transformation from the amorphous form to the crystalline form [60-62].

3.1.2. Modification by chemical reactions

There are various pathways or processes designed to incorporate chemical species onto the porous materials for different purposes related to their function or use after they are synthesized. The process of such incorporation may be termed grafting as the attached chemical species are added to stabilize the porous materials in solution, for adsorption or for anchoring other chemicals. Nawrocki et al. [14, 15] listed three classes of surface modifications as dynamic modification, permanent modification and physical screening.

a) Physical screening

This method involves a deposition of a thin layer of polymer on the surface of the metal oxide (e.g. silica) to improve its chemical and pH stability. This is very useful in chromatography where packing materials such as microporous silica and alumina may possess excellent separation and selectivity properties but deficient because of limited chemical and pH stability. The polymeric layer therefore shields the surface of the metal oxides from interactions with aggressive eluents while the porosity and thermal stability of the materials remain intact [63, 64]. The method of immobilization of the polymeric layer is physisorption. The polymer layer is adsorbed to the surface of the material without chemical bonding.

b) Dynamic modification

In this method chemical species are indirectly added onto the surface of a metal oxide with the aim of covering unwanted sites on the metal oxide surface or generation of a temporarily bonded phase on the surface. The modifying chemical species are introduced to the surface via a medium through which the modifying species will interact with the surface of the metal oxide. These interactions lead to blocking of acid/basic sites on the metal oxide surface [65] or hinders unwanted interactions with the surface. For example, addition of lactic acid in phosphopeptide enrichment procedures hinders the interaction of unphosphorylated proteins with the metal oxide surface [66]. The modification is termed dynamic because the modifying species form a temporary bonded phase with the metal oxide surface.

c) Permanent modification or functionalization

This modification involves coupling of the chemical species to the surface of the metal oxide via a chemical reaction. The interaction of the chemical species with the metal oxide surface may be electrostatic (as a result of the charges on the surface of the metal oxide), or covalent bonding via surface polymerization. Procedures such as binding of carboxylate ligands, silanes and phosphate groups are examples of permanent modifications [7, 67]. The duration of the so-called permanent modification is however questionable as will be seen in the results section.

The dominant groups on metal oxide surfaces are hydroxyls which are abundant on most metal oxide surfaces. The surface hydroxyls of inorganic oxides are sufficiently acidic for reaction with most organometallic compounds. There are also the metal-oxo-metal groups (M-O-M) which can be amphoteric with anion and cation exchange properties depending on the metal bonded to the -OH group. Most functionalization techniques are based on the reaction of the surface hydroxyl with the functional group of the coupled chemical species. Metal oxides have been functionalized with different chemical species such as carboxylate ligands, amines, silanes and phosphonates and other functional groups for various purposes [1]. For example salinized zirconia has been used in chromatography [15, 68] and surface functionalized nanoparticles in photo catalytic applications [69]. There are numerous schemes with different strategies, but most of them follow the route of anchoring a functional group to the metal oxide surface through a binding group or a linker. For example, a binding group such as a silane is used to link a functional group like an amine to the surface of the metal oxide. Other functional groups such as thiols, disulfides, carboxylic acids, etc. can also be used [7]; the choice depends on the purpose of the functionalization. In Figure 9, the scheme shows the aminopropylethoxysilane (APTES) functionalization of a metal oxide. The binding group is the silane part which anchors the amine part onto the surface of the metal oxide.

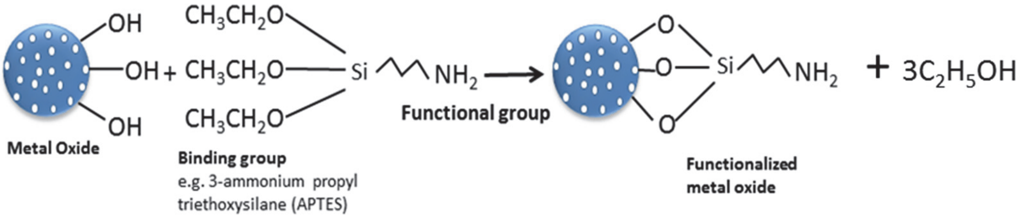

Figure 9: Metal oxide functionalization scheme.

There are many functionalization methods similar to the one shown above, used to attach functional molecules to metal oxides. Examples include the modification of TiO_2 and ZrO_2 with organosilanes and organophosphonates[70] as well as the adsorption of polyelectrolytes on TiO_2 and SiO_2[71]. The M-O-P bond formed between the metal oxide surface and the phosphonate is stable to hydrolysis. Consequently, organophosphonate-modified metal oxides are used in applications such as protein immobilization [67]. The adsorption of polyelectrolytes such as polyvinylpyridine is based on electrostatic attraction between the polymers and the hydroxyl groups on the metal oxide surface. These interactions are utilized in waste water treatment.

There are also methods where the functional group on the metal oxide serves as a linker to another functional group, as shown by Wu et al. [24, 72]. A bifunctional alkoxysilane (3-mercapto-propyltrimethoxysilane) bearing a sulfonate group was linked to a TiO_2 film on one end and a glass substrate on the other end. The silane part of the molecule 'holds' the surface of the substrate by molecular self-absorption while the sulfonate connects the metal oxide. The silane enhanced the adherence of the TiO_2 film to the substrate, and the sulfonate aided the dispersion of the TiO_2 particles thereby improving the penetration of UV light and oxygen.

4. APPLICATIONS IN SEPARATION

Porous metal oxides are widely applied in adsorption and molecular separation [8, 14, 15]. The well-defined pore structure, narrow pore size distribution and large surface areas coupled with the unique surface chemistry of porous metal oxides are utilized in the adsorption and separation of biomolecules such as proteins and phospholipids. Due to the high chemical stability of porous metal oxides, they are able to withstand a wide pH range. Secondly, they are thermally stable and are thus able to tolerate high temperatures. Properties of metal oxides such as the isoelectric point (IEP) and acidity/basicity play active roles in adsorption.

Liquid chromatography (LC) is a common separation technique which has gone through various developmental stages including the development of high performance liquid chromatography (HPLC) since the late 1960s when microporous particles became available [73]. There are different types of liquid chromatography based on the column material, mode of operation and the purpose. The column materials in liquid chromatography are usually porous and the separation mechanism based on the interaction of the porous materials with the mobile phase. For example in the HPLC, the column is packed with porous metal oxide beads such as silica or zirconia modified with organic compounds like n-octadecyl, n-octyl groups or polymeric compounds such as polystyrene or polybutadiene. The modification was to improve the chemical stability of the metal oxides and reduce access to Lewis acid sites [14, 15]. More recent examples of chromatographic techniques include capillary liquid chromatography (CLC), capillary electrochromatography (CEC) and metal oxide affinity chromatography (MOAC). CLC has smaller column internal diameter and a lower eluent rate compared to conventional HPLC, this saves solvents, reagents and packing materials [74]. However, CEC is a combination of two analytical techniques namely HPLC and capillary electrophoresis. However in MOAC, the columns are packed with porous metal oxides and the separation is based on the interactions of the metal oxide surface with the mobile phase.

Silica has been the foremost choice of porous material for column packing [14]. Although silica has been modified and functionalized with an appreciable level of success [1, 75-77], there are some drawbacks with silica material. These drawbacks include poor chemical stability of the porous materials and poor separation efficiency. Porous metal oxides such as zirconia, titania and alumina have shown better performance with improved stability and better separation efficiency. These metal oxides are thus alternatives to silica as traditional chromatographic material [14, 15, 68]. In this thesis, the porous metal oxide materials synthesized were applied to CLC, CEC, and MOAC.

4.1. Electrochromatography

The driving force for separation in capillary electrochromatography is the electric field rather than pressure as in the case of regular LC. It combines the advantages of HPLC and electrophoresis, and is used as a variant of HPLC. The CEC capillaries are packed with porous microparticles and electrophoresis occurs as the mobile phase is electroosmotically driven through the chromatographic bed [78-81]. The electroosmotic flow is generated by a large voltage applied along the length of the column (see Figure 10). The added electrolytes cause positive ions to accumulate in the double layer of the particles of column packing. The ions then move towards the cathode thus dragging the liquid phase along and causing the desired separation. The separation is a result of attractions based on the charges on the microparticles. [82].

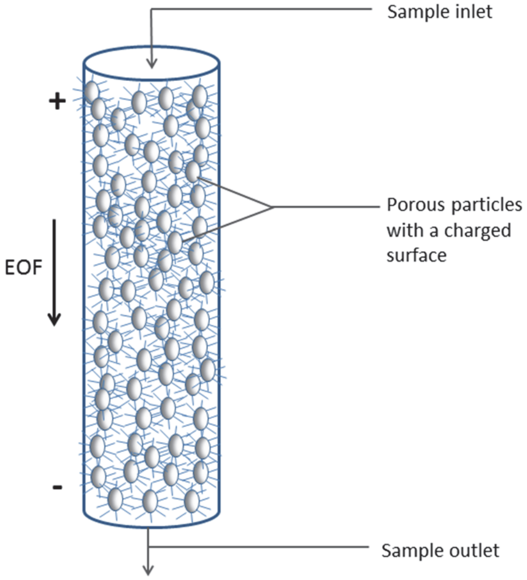

Figure 10: Pictorial representation of the electrochromatography process.

4.2. Phosphopeptide enrichment

Another kind of chromatographic technique is metal oxide affinity chromatography (MOAC). MOAC is a widely used analytical tool in phosphoproteomics. It is based on the interaction of metal oxides with the phosphate group of phosphorylated proteins [66]. It is a prominent method used to enrich phosphopeptides before they are analyzed by liquid chromatography-mass spectrometry (LC-MS).

Identifying and localizing phosphorylation sites are key to understanding cellular signaling cascades and other biological networks [8]. Identifying phosphorylation sites is however not a straight forward procedure as only a small number of proteins can be identified with technologies such as radioactive labelling and gel electrophoresis[66]. The development of new technologies such as modern mass spectrometry and improvement in computing facilities has allowed the handling of considerably larger amount of proteins. New protocols and techniques have also been developed and these have consequently led to the development of a specialization known as phosphoproteomics

[83, 84]. Increased scan speeds and commercial availability of high-resolution hybrid mass spectrometers have raised both the quantity and quality of data acquired. Despite all these recent developments, phosphorylation sites cannot be adequately identified and quantified without resorting to an enrichment procedure. Phosphopeptide enrichment protocols are methods used to reduce the complexity of the peptide mixture in order to ease later analysis and allow the identification of phosphorylation sites.

TiO_2 and ZrO_2 are the two metal oxides most commonly used as phosphopeptide enrichment material [83, 84]. Other metal oxides such as Al_2O_3 [85], Fe_2O_3 [86], Ga_2O_3 [87], SnO_2 [8, 66, 88] and recently materials with perovskite structures such as $CaTiO_3$, $SrTiO_3$, $MgTiO_3$, $BaTiO_3$ and $CaZrO_3$ [89] have also been shown to be promising phosphopeptide enrichment materials. Metal oxides are used as enrichment materials because of their phosphate affinity. They possess Lewis acid and ion exchange properties which enable them to bind to phosphate groups at certain acidic conditions and elute at alkaline conditions.

In phosphopeptide enrichment, as shown in Figure 11, the protein mix is digested and fragmented into peptides and purified. The digestion and fragmentation loosen the proteins which may be rigid and tightly bound. The proteins are then broken down into smaller peptides which are easier to handle. The purification step is carried out to remove thiol groups because free thiol groups can lead to unpredictable oxidation such as oxidation to sulfonic acid or formation of disulfide bonds which in turn makes the proteins rigid and difficult to cleave.

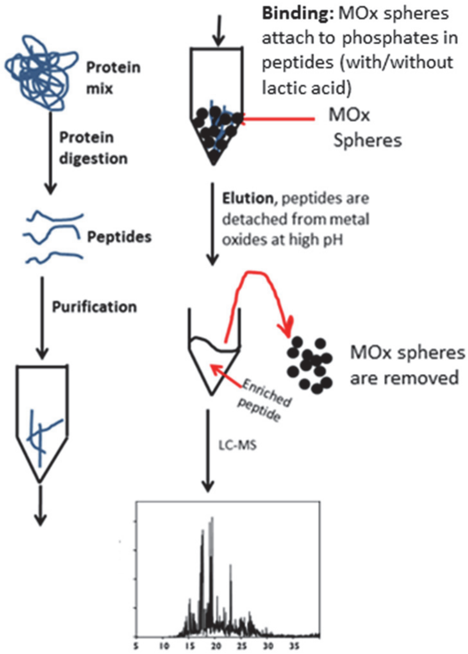

Figure 11: A typical phosphopeptide enrichment protocol.

The purified peptides are then added to pre-washed metal oxide particles and the pH is adjusted to acidic conditions (pH ~2) for binding the phosphopeptides. At acidic conditions, the peptides bind to the metal oxides and they are eluted at high pH (~10). After the elution, the metal oxides are removed by centrifugation and the enriched peptides are then analyzed by LC-MS. Further analyses are then continued with other analytical tools and specific database. Results such as the number or amount of phosphorylation sites and the type of phosphorylation i.e. singly phosphorylated (1P) or multiply phosphorylated (2P, 3P, 4P or 5P) peptides are obtained from these analyses.

5. AIMS OF THE STUDY

One of the objectives of this thesis is to point out the crucial steps in the nanocasting process and examine how to control these steps in order to obtain successful replicas. Furthermore, the functionalization and subsequent application of successful metal oxide replicas in separation processes is studied.

In an ideal nanocasting scheme, the replicas are supposed to be a negative cast of the template. This is to say the textural and morphological properties of the replicas should directly correspond to that of the template. This is however not observed in some cases for various reasons. This thesis points out some of these reasons with the aim of improving the understanding of the processes in the nanocasting scheme and to show how controlling these processes will lead to the production of successful replicas.

Functionalization is crucial in some applications of the porous metal oxides. Therefore after successfully synthesizing the metal oxides, the second objective of the thesis is to study some surface interactions and functionalization of the metal oxide replicas. The hydrolytic stability of these interactions will also be studied. The functionalized metal oxides will then be tested as chromatographic materials. The objective of the thesis at this point is to test whether nanocast metal oxides can be viable alternatives to traditional chromatographic column materials like silica and to highlight the benefits of nanocast metal oxides as chromatographic materials.

The third aim of this thesis is to study the application of nanocast metal oxides in another separation process i.e. phosphopeptide enrichment. This study compares the performance of different nanocast metal oxides in enrichment procedures. By using the nanocasting process materials with comparable morphological and structural properties can be studied. Moreover this study will include an investigation of the surface chemistry and binding characteristics of these materials in a bid to aid the identification of phosphorylated peptides, thereby enabling the optimization of the enrichment protocols and materials.

6. EXPERIMENTAL

6.1. Silica templates

All silica templates used were commercially obtained except for SBA-15 which was synthesized in the laboratory.

6.1.1. Commercial templates

The silica materials tabulated below were obtained commercially and used in the synthesis of the metal oxides.

Silica Template	Manufacturer	Particle size (µm)	Pore size (nm)	Morphology
LiChroprep Si 60	Merck	5-20	10	Irregular
Shiseido EP-DF-5-120 Å	Shiseido	5	12	spherical
Daisogel SP-120-10P	Daiso	10	12	spherical
Daisogel SP-300-10P	Daiso	10	30	spherical

6.1.2. Preparation of the SBA-15 template material

Mesoporous SBA-15 was synthesized following the procedure described by Choi et al. [40]. Pluronic P123 (5.2 g) was dissolved in 94.4 mL deionized water (Millipore) containing 2.8 g HCl (37%). 11.16 g of tetraethoxysilane (TEOS) was added under vigorous stirring for 24 h, after which the sample was hydrothermally treated at 90 °C for 24 h. The precipitate was later filtered and dried at 90 °C. The organic template was then removed by extraction by adding 126.7 mL ethanol and a few drops of HCl and stirred at room temperature for half an hour followed by filtration. Finally, the material was calcined by heating to 120 °C for 2 h, and up to 550 °C for 5 h and then kept at 550 °C for another 2 h.

6.2. Nanocasting of metal oxides

The method of nanocasting was used to synthesize all the non-siliceous metal oxides used in this work according to four main protocols:

6.2.1. Synthesis of TiO_2 microspheres

The TiO_2 microspheres were made according to the following protocol. 1.5 mL titanium isopropoxide was dissolved in 1.5 mL ethanol, after which the solution was added to 0.25 g of silica. The suspension was stirred at 500 rpm for about 4 h and then centrifuged at 3000 rpm for 2 min to remove the supernatant, and then dried at 95 °C overnight. The impregnated silica particles were then mixed with 1.5 mL ethanol and 1.5 mL water and stirred for 4 h at 500 rpm. The suspension was centrifuged again and then dried at 150 °C overnight. The impregnation-heating cycle described above was repeated once more and then the dried particles were calcined using the following heat ramp: 150 °C for 3 h, 250 °C for 3 h, 550 °C for 5 h with a heating rate of 1 °C/min. In the final etching step, 2 M NaOH was added to the calcined particles and was heated at 80 °C overnight. The etching process was repeated once more, then the particles were centrifuged and washed, first with water and then with ethanol before drying at 70 °C. In some cases where the surface area is required to be within a specific range (Paper IV), the TiO_2 microspheres were further calcined after etching. Additional calcination was done at 650 °C for 2 h at the same heating rate of 1 °C/min in order to partially sinter the material.

6.2.2. Synthesis of ZrO_2 microspheres

For the preparation of ZrO_2, 0.5 g $ZrOCl \cdot 8\ H_2O$ was dissolved in 0.5 g H_2O. Then 0.25 g silica was added to the solution and stirred for 1 h at 500 rpm. The mixture was centrifuged at 3000 rpm and the supernatant was removed. The impregnated spheres were heated at 70 °C overnight and calcined as follows: 150 °C for 3 h, 250 °C for 3 h, and 550 °C for 5 h with heating rates of 1 °C/min. This process was repeated two times more before etching twice in 2 M NaOH solution at 80 °C overnight, followed by washing with water and ethanol, and then drying at 70 °C.

6.2.3. Synthesis of SnO_2 microspheres

For the preparation of SnO_2, 1.35 g of $SnCl_2$ was dissolved in 0.75 mL H_2O, to which 0.25 g silica was added and stirred for 1 h at 500 rpm. The mixture was centrifuged at 3000 rpm and the supernatant subsequently removed. The impregnated spheres were heated directly at 150 °C for 3 h, then at 250 °C for 3 h, and finally at 550 °C for 5 h with a heating ramp of 1 °C/min. The silica template was finally etched using 2 M NaOH solution at 80 °C two times and dried at 70 °C.

6.2.4. Synthesis of Fe_2O_3, Co_3O_4, NiO, and In_2O_3 microspheres

Fe_2O_3, Co_3O_4, NiO, and In_2O_3 microspheres were all synthesized from hydrated nitrate salts using the double solvent method wherein a pre-determined amount (calculated from the total pore volume of silica) of the nitrate salt solution is added to the silica particles earlier dispersed in n-hexane. For example, in the synthesis of Fe_2O_3, 0.25 g of silica was dispersed in 2 mL of n-hexane and stirred at 500 rpm. 300 μL of a 2 M solution of iron nitrate nonahydrate was added to the suspension with continuous stirring for 1 h after which the n-hexane was removed. The resulting wet particles were allowed to dry at room temperature for about 4 h, after which they were heated as follows: 140 °C for 1 h, and then 300 °C for 2 h, at a heating rate of 1 °C/min. This impregnation step was repeated 10 or more times (in order to obtain well-defined and smooth particles), after which the particles were calcined at 550 °C for 5 h with a heating rate of 1 °C/min. Thereafter, the particles were etched twice in 2 M NaOH solution at 80 °C. For Co_3O_4, NiO and In_2O_3, a similar procedure was followed but 3 M solutions of cobalt nitrate hexahydrate, nickel nitrate hexahydrate, and indium nitrate hydrate were used for same amount of silica particles.

6.2.5. Impregnation of SBA-15 with $Ni(NO_3)_2 \cdot 6H_2O$ salts

The SBA-15 material was impregnated with nickel nitrate salt using a similar "wet impregnation" technique as described by Tian et al. [36]. 1.0 g of SBA-15 material was added to a solution of 3.39 g nickel nitrate hexahydrate ($Ni(NO_3)_2 \cdot 6H_2O$) dissolved in 33.3 g absolute ethanol. Ultrasonication was used to ensure complete wetting of all pores. The ethanol was slowly evaporated under vacuum at room temperature for 12 h using a cold trap and then transferred into a crucible and dried at 70 °C under vacuum for another 48 h (this sample is referred to as Ni-dried). The SBA-15/nickel nitrate composite materials were calcined in air or in helium up to 140 °C, 200 °C, 300 °C, and 500 °C after which the samples were cooled down again. The gas flow for each gas used was about 20 mL/min and the heating ramp was 2 °C/min.

6.3. Amino-modification of SiO_2, SnO_2, TiO_2 and ZrO_2

All samples were exposed to plasma cleaning (Harrick plasma cleaner/sterilizer PDC-32G) for 5 minutes to ensure the complete removal of organic residue from the surfaces. The different modification compounds are depicted in Figure 12.

(3-Aminopropyl)triethoxysilane 2-Aminoethyl dihydrogen phosphate

Aziridine (ethyleneimine) Polyethyleneimine

Figure 12: Molecular structures of the different modification agents.

6.3.1. 3-Aminopropyltriethoxysilane-modification (APTES)

0.1 g of the SiO_2, TiO_2, and ZrO_2 particles and 0.32 g SnO_2 were degassed at 70 °C for more than 6 h to remove residual physisorbed water. Under inert argon atmosphere, anhydrous toluene (1.7 mL) was added to the particles together with a specific amount of APTES scaled to the total surface area of the different samples (i.e. 42 µL for SiO_2, 25 µL for TiO_2, 18 µL for ZrO_2, and 17 µL for SnO_2). The mixtures were then refluxed at 110 °C overnight. They were thereafter washed 3 times with toluene and dried at room temperature in a vacuum oven. These samples are denoted MO_2-APTES, where M = Si, Ti, Zr, or Sn depending on the metal oxide.

6.3.2. Aminoethyldihydrogen phosphate modification (AEDP)

The AEDP-modification was done in accordance to the protocol described by Myller et al. [90]. 0.1 g of each of the SiO_2, TiO_2, and ZrO_2 particles and 0.32 g of the SnO_2 sample were dispersed in 0.01 M aqueous solution of AEDP. The dispersion was mixed overnight, washed two times with water and once with ethanol and dried at 120 °C overnight. These AEDP-modified samples are denoted MO_2-AEDP, where M = Si, Ti, Zr, or Sn depending on the metal oxide.

6.3.3. Surface polymerization using aziridine (AZ)

A hyperbranched PEI-modification of the metal oxide particles was made by surface polymerization of aziridine according to earlier described protocols [91]. Prior to the reaction, 0.1 g of the SiO_2, TiO_2, and ZrO_2 particles and 0.32 g SnO_2 were degassed at 70 °C for more than 6 h to remove residual physisorbed water. Under inert argon atmosphere, anhydrous toluene (15 mL) was added to the particles together with catalytic amounts of acetic acid and certain amounts of aziridine (70 µL for SiO_2, 40 µL for TiO_2, and 27 µL for ZrO_2 and SnO_2). The mixtures were then refluxed at 75 °C overnight. After the polymerization reaction was completed, the sample was washed 3 times with toluene and 3 times with methanol and then dried in a vacuum oven at room temperature. These samples are denoted MO_2-AZ, where M = Si, Ti, Zr, or Sn depending on the metal oxide.

6.3.4. Modification with polyethyleneimine (PEI)

The final surface modification method entailed the use of PEI by electrostatic coupling. In four different sample tubes, 0.89 g of PEI was dissolved in 10 mL water and 0.1 g SiO_2, TiO_2, and ZrO_2 as well as 0.32 g SnO_2 were added. The mixtures were stirred overnight. The particle were thereafter washed twice with water and once with ethanol and dried at 50 °C overnight. These samples are denoted MO_2-PEI, where M = Si, Ti, Zr, or Sn depending on the metal oxide.

6.4. Quantification of amino groups

The amount of accessible primary and secondary amino groups was determined spectrophotometrically by using the ninhydrin method as described by McCaldin [92] and widely used for amino group determination. A standard curve was made using APTES as the model because it has only one primary amino group per molecule. Afterwards, 2 mL of ninhydrin solution (3.5 mg/mL in absolute ethanol) was added to 0.5 mg of metal oxide sample (except for SnO_2, for which 1 mg was used). The samples were heated at 95 °C for 8 min and the absorbance was measured at 585 nm wavelength on a spectrophotometer.

6.5. Hydrolytic stability tests

The chemical stability of the functionalized materials was verified by measuring the zeta potential in 10 mM *N*-2(2-hydroxyethyl)piperazine-*N*´-2-ethanesulfonic acid (HEPES) solution (pH~7.2) after the materials had been aged for different time intervals of 0, 6, 20 and 40 h at pH 2 and pH 10 adjusted with 0.05 M HCl and 0.05 M KOH, respectively.

6.6. Materials characterization

6.6.1. X-ray diffraction and small angle x-ray scattering

X-ray diffraction (XRD) and Small angle x-rays scattering (SAXS) belong to a group of x-ray techniques widely used to study structural features on the nanometer level. A combination of diffraction and scattering can provide extensive information about the microstructure of porous materials as well as the nature and properties of the crystalline material absorbed within the pores. Both techniques provide similar information about the structure of the sample but on different length scales. XRD has a wider angle of scattering compared to SAXS and can provide information about the phase, unit cell dimensions, distance between layers or rows of atoms and crystal sizes. SAXS can be used to study non-homogeneous systems with sizes between 1-100 nm within 0.1 and 10° scattering. The shape and size of macromolecules as well as the characteristic distances of partially ordered materials and pore sizes are some of the information obtained through SAXS measurements. Figure 13 gives a comparison of the two techniques.

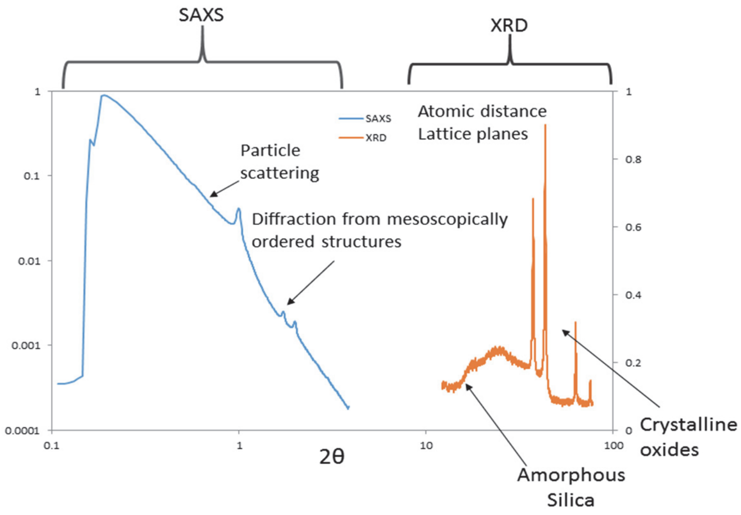

Figure 13: Pictorial representation of the SAXS and XRD techniques.

When an x-ray beam with wavelength λ strikes a material with periodic long range order, characteristic reflections of the diffraction pattern are observed as a result of the constructive interference when the glancing angle θ satisfies the Bragg's law:

$$n\lambda = 2d \sin\theta \tag{6.1}$$

where d is the repeating distance between the reflecting planes and n is an integer number[93]. Bragg's law shows the relationship between crystal lattices d, and the reflection angle observed as illustrated in Figure 14. The scattered intensity is measured with respect to the scattering angle θ.

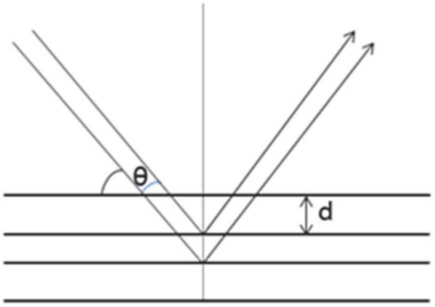

- Θ is the glancing angle

-***d*** *is the repeating distance between the reflecting planes*

- ***n*** *is an integer number*

Figure 14: Schematic representation of Bragg diffraction.

There are seven unique crystal arrangements, namely, cubic, hexagonal, tetragonal, orthorhombic, rhombohedra, monoclinic and triclinic. The scattering pattern of a compound depends on the arrangement of its unit cells and lattice spacing, therefore each structure has a unique scattering or diffraction pattern characterized by a particular *d*-spacing and scattering intensity. By analyzing these scattering patterns, size, shape and the electron density distribution can be obtained.

Small angle x-ray scattering is an elastic scattering in a material and it corresponds to the electron density contrast which is the physical property that is being measured. The scattering process may be described as shown in Figure 15. The incident x-rays are scattered from the two indicated points at angle 2θ with a path length of 1λ between them. The electrons resonate with the frequency of the x-rays passing through the objects and emit coherent secondary waves which interfere with each other.

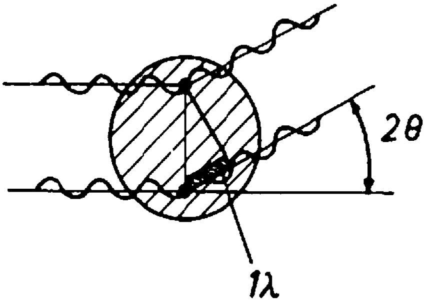

Figure 15: x-ray scattering of incident waves (from [93]).

SAXS and XRD can be used for *in-situ* and *ex-situ* studies, both have been used in this work. The *ex-situ* SAXS measurements were carried out with a Kratky compact small angle system (Hecus, Austria). The system is equipped with a position sensitive detector (PSD 50M) consisting of 1024 channels of 55.5 μm width each. A Seifert ID-300 X-ray generator, operating at a maximum intensity of 50 kV and 40 mA, provided the Cu Kα radiation at $\lambda = 0.1542$ nm. The sample-to-detector distance was 277 mm and the exposure time was 600 s for each sample. The sample holder was kept under vacuum during the measurements to minimize the background scattering from air. The ex-situ XRD measurements were carried out on a Bruker AXS D8 Discover with a HI-Star 2-D detector using a Cu Kα X-ray source. The Scherrer's equation was applied to estimate crystallite sizes of the different metal oxide composites, etched metal oxides and silica materials [27].

In situ characterization techniques were applied to obtain a clearer picture on the evolution of the nickel nitrate and oxide inside the pores of the SBA-15 template. *In situ* XRD and SAXS measurements were carried out at the Elettra synchrotron beamline facility (Trieste, Italy). The XRD data was recorded in the range of 26.0–42.5° with a 1D Gabriel type gas detector, while the SAXS data was collected using a 2D Pilatus100K Detector System with the camera length of 1.5 m and in the *q* value range of 0.08-2.75

nm^{-1}. A gas blower system for x-ray and neutron studies (Oxford Danfysik DGB-0002) was used to heat the sample in a capillary tube up to 500 °C with a ramp of 2 °C/min (in both air and He gas flows).

6.6.2. UV-vis spectroscopy

Ultra-violet - visible light (UV-vis) spectroscopy is a method based on the interaction of light with the matter of interest in the UV-vis wavelength range. In UV-vis absorption spectroscopy, the attenuation of a beam of light after it passes through a sample or after its reflection from a sample surface is measured. When the electromagnetic radiation is absorbed by matter, the energy of the photon is converted to internal energy which is measured at a particular wavelength or over a range of wavelengths. The absorption is based on the Beer-Lambert law [94] which shows that there is a linear relationship between the transmittance and intensity of electromagnetic radiation. The transmittance (T) is mathematically expressed as:

$$T = \frac{I}{I_o} = e^{-\alpha' l} = e^{-\sigma l N} \tag{6.2}$$

where I_0 and I are the intensity (power per unit area) of the incident light and the transmitted light, respectively; σ is the cross section of light absorption by a single particle and N is the density (number per unit volume) of absorbing particles. The absorbance can be calculated from transmittance by equation 6.3:

$$A = -log_{10} \frac{I}{I_0} \tag{6.3}$$

The absorbance is linearly dependent on the concentration (or number density of absorbers) according to

$$A = \epsilon lc = \alpha l \tag{6.4}$$

Beer-Lambert's law can be applied to most dilute solutions, $c \leq 0.01$ M. At high concentrations deviations from the law can be observed due to changes in the absorbing species or the properties of the bulk solution [94]. Therefore, a good way of studying the interaction between two molecules or the progression of a chemical reaction is to observe the changes in UV-vis absorption before and after the reaction. This can be used to measure the amount of moles adsorbed or desorbed, and hence deduce the adsorption/desorption properties and type/mode of reaction. For example in this work, UV-vis was used to quantify the amount of amino groups adsorbed on the surface of selected metal oxide microparticles by using the nyhindrin method [92].

The equipment used in this work was a Nanodrop 2000c Thermo Scientific spectrophotometer.

6.6.3. Infrared spectroscopy

Molecules vibrate in a distinct manner that is characteristic of their structure. The infrared (IR) light can be used to excite molecules and the wavelengths of the absorbed IR light correspond to the characteristic vibrational-rotational structure of the material. The molecules may rotate around their axis of symmetry or the two perpendicular axes while vibrations can be in the form of bending or stretching of the bonds. The frequency of the vibrations is associated with a particular normal mode of motion and a particular bond type. The different modes of vibration are symmetric and asymmetric stretching, scissoring, rocking, wagging and twisting, etc. Modern spectrometers operating in the infrared and near infrared regions use Fourier transform techniques for spectral detection and analysis and are therefore named Fourier Transform Infrared (FTIR) spectrometers.

Different parts of a molecule (e.g. hydrocarbon backbone, functional groups or radicals) have a signatory vibrational frequency which occurs at a particular wave number. This can be used to identify the presence of such parts of a molecule or functional groups in a sample. In this work FTIR spectroscopy was used to confirm the presence of amino groups, phosphate groups, and other groups adsorbed on the metal oxides.

The spectrophotometric instrument used in this study was Perkin Elmer Paragon 1000 FTIR spectrometer.

6.6.4. Zeta potential measurements

When two phases are in contact, a difference in potential usually develops between them. In aqueous solutions for example, the dipolar molecules of water tend to be oriented in a particular direction at the interface. Ions in solution or excess electrons from the other phase (for instance, metal oxide particles) interact with the water molecules and this leads to a potential difference. The interaction forces at this interface may be analyzed in terms of the electrostatic potential by calculating the average potential in the surface of shear. This is termed the zeta potential symbolized universally with the Greek letter zeta (ζ) [95].

The zeta potential is a physical property which is displayed by any particle in a suspension. When a charged particle is suspended in liquid, oppositely charged ions are attracted to the surface of the particle. The movement of ions at the surface affects the charge distribution in the regions close to the surface thereby increasing the concentration of counter ions close to the surface. This leads to the formation of an 'electrical double layer' at the region of the particle-liquid interface as shown in Figure 16. The top part of Figure 16 shows an inner region which includes the ions bound closely to the surface and an outer region where a balance of electrostatic forces and random thermal motion control the distribution of ions [96].

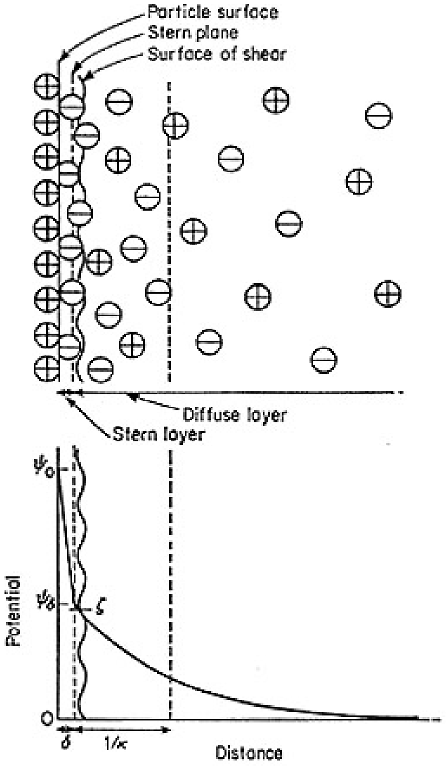

Figure 16: Schematic representation of the electric double layer based on Stern's theory [97].

The potential at this region decays as the distance increases from the surface until it reaches a distance at which the value becomes the same as in the bulk solution which is conventionally assumed to be zero as shown in the lower part of Figure 16.

The zeta potential relates the surface charge of the particle, as well as any adsorbed layer at the interface to the nature and composition of the surrounding medium. One significant use of the zeta potential is that its magnitude gives an indication of the stability of a colloidal system. When the particles in a system have a large negative or positive ζ potential, they repel each other and therefore do not tend to flocculate. The value of the ζ potential generally accepted for stability is ± 30 mV. However, as the ζ potential changes with pH, electrophoresis may be used to determine the isoelectric point (IEP). This is the pH at which the net effective surface charge is zero and is also the point at which the colloidal system is least stable [98]. The ζ potential can also be used to confirm specific adsorption on the surface of particles as a shift in the ζ potential either positively or negatively in the IEP indicate the presence of adsorbed species depending on the nature of the species adsorbed.

In this study, the ζ potential measurements were made using a Zetasizer NanoZS instrument (Malvern Instruments) based on electrophoresis.

6.6.5. Nitrogen physisorption

Nitrogen sorption is a technique widely used for characterization of porous materials. This technique can be used to measure a wide range of pore sizes from 0.35 nm up to 100 nm thus including micropores and mesopores [97].

Adsorption is the enrichment of one or more components in the interfacial layer. In nitrogen sorption, the interface is a gas/solid interface, in which the solid (the material to be characterized) is the adsorbent, the gas which is absorbed (in this case nitrogen) is the adsorptive and the fluid (which is liquid nitrogen) is called the adsorbate [34]. The amount adsorbate adsorbed on a solid surface is controlled by the absolute temperature *T*, the pressure *P* and the interaction potential *E* between the vapor and the surface. The nitrogen sorption technique can be used to determine the surface area, pore size distribution and pore volume of porous materials.

In a typical nitrogen sorption measurement, the results are usually plotted as an isotherm i.e. the volume of gas adsorbed against the relative pressure P/P_0 at a constant temperature (usually 77 K). Such isotherms may also contain adsorption and desorption parts which can be used to describe the porous material after subsequent analysis of the isotherm. There are six main types of isotherms according to the IUPAC classification (see Figure 17).

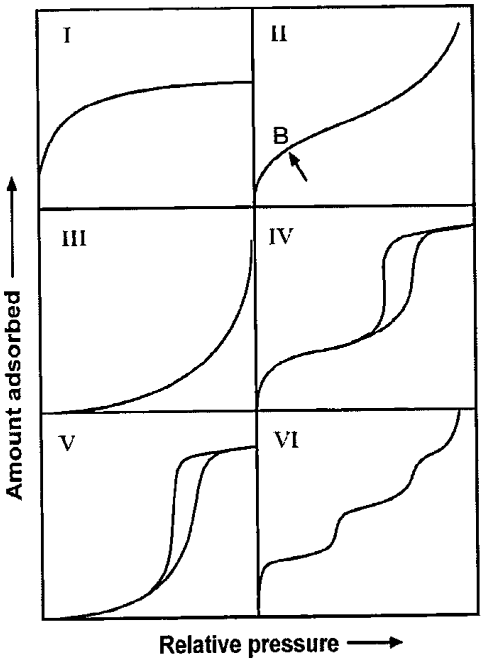

Figure 17: Six main types of adsorption isotherms according to the IUPAC classification (from [34]).

All adsorption isotherms should fit at least one of the classes. From the adsorption isotherms one can see the interaction between the adsorbate and the adsorbent as well as the type of porosity (porosities) of the sample [97].

The *Type I* isotherms are obtained when the adsorption is limited to a few molecular layers, and are relevant for microporous materials which is seen by the high uptake at relatively low pressures due to the narrow pore width and high adsorption potential of the micropores. *Type II* isotherms are obtained when the adsorbent is non-porous or macroporous. In this case there may be unrestricted monolayer-multilayer adsorption. There is also an inflection point B which indicates the point of completion of monolayer coverage and the beginning of multilayer adsorption. *Type III* isotherms are for materials in which the adsorbate-adsorbent interactions are weak and the adsorbate-adsorbate interactions are relatively strong. *Type IV* isotherms are typical for mesoporous materials. Its distinguished feature is the hysteresis loop which is a result of the occurrence of capillary condensation inside the mesopores. The adsorbate uptake occurs over a range of P/P_0 and ends in a plateau of the isotherm, which shows that pore filling is complete. The beginning of the *Type IV* isotherm can be attributed to monolayer-multilayer adsorption as was the case in *Type II isotherms*. *Type V* isotherms also show pore condensation and hysteresis, however the initial part of these isotherms are similar to *type III* isotherms where weak interactions occur between adsorbate and adsorbent. *Type VI* isotherms can be considered a special case because stepwise multilayer adsorption occurs on a uniform, non-porous surface [34]. The powders studied in this work showed mainly *type IV* isotherms. The *specific surface area* was determined by the BET (Brunauer, Emmett and Teller) method obtained from the nitrogen physisorption data. Other useful data obtained from the nitrogen physisorption measurements were the *pore volume*, *pore size* and *pore size distribution* which are described below.

(a) BET surface area

Application of the BET equation is the most popular approach to the calculation of the specific surface area of solid materials [34]. The equation is derived from the Langmuir theory which is a kinetic model of monolayer adsorption on an array of identical sites. The original BET equation is essentially a multilayer extension of the Langmuir theory, the adsorbent is seen as an array of equivalent sites on which molecules are randomly adsorbed. It also assumes that the probability that an adsorption site is occupied does not depend on the occupation of the neighboring sites and that there are no lateral interactions between the adsorbed molecules. The BET equation is usually applied in its linear form as:

$$\frac{{}^{p}/_{p_0}}{n\left(1-{}^{p}/_{p_0}\right)} = \frac{1}{n_m C} + \frac{(C-1)\cdot p}{n_m C\cdot p_0} \tag{6.6}$$

n is the amount adsorbed at the relative pressure P/P_0 and n_m is the monolayer capacity.

The constant *C* in the equation is related to the sharpness of the point *B* indicated in Figure 17 (*II*) and the value is sensitive to the surface polarity and/or to the presence of microporosity. *C values* are normally between 50 and 200 in *Type IV* isotherms, 50 is considered hydrophobic while 200 is considered hydrophilic [34]. The BET surface area is then calculated from the monolayer capacity n_m as:

$$A_s\ (BET) = n_m \cdot N_A \cdot a_m \tag{6.7}$$

and

$$a_s\ (BET) = A_s(BET)/m \tag{6.8}$$

Where a_m is the average area occupied by each molecule in the monolayer, A_s (BET) and a_s (BET) are the total and specific surface areas respectively of the adsorbent of mass *m* and N_A is the Avogadro's constant. The BET method is strictly applicable for assessment of non-porous, mesoporous and macroporous materials [98].

(b) Pore size analysis

The commonly used methods for analyzing pore sizes and pore size distribution are based on the Kelvin equation [34]. The Kelvin equation relates the equilibrium vapor pressure of a curved surface, such as that of a liquid in a capillary or pore (*P*), to the equilibrium pressure of the same liquid on a planar surface (P_0). For a cylindrical pore the Kelvin equation is given as:

$$\ln \frac{P}{P_0} = \frac{2\gamma V_m}{r_K RT} \tag{6.9}$$

where γ is the surface tension , V_m is the molar volume of the condensed liquid and r_K is the mean radius of the meniscus. The Kelvin equation shows the relationship between P/P_0 and r_K is the mean radius of the meniscus of the liquid. *R* is the gas constant and *T* is the temperature. Another model used for calculating the pore size distribution is the Barrett-Joyner-Halenda (BJH) model. It is based on the Kelvin-Cohan equation and may be used to estimate and compare pore sizes of different materials although its accuracy is limited [99]. Another method commonly used is the Density Functional Theory (DFT) method which is based on statistical mechanics. In the DFT method, equilibrium density profiles of all points inside the pore are obtained by minimizing the free-energy functional. The free energy potential also contains other interactions such as the attractive and repulsive interactions from the fluid-fluid and fluid-wall interactions which may be obtained from the non-local density functional theory (NLDFT) [34, 100]. The pore size distribution is obtained by comparing the experimental isotherm obtained from the nitrogen sorption measurement with the isotherm determined by the NLDFT.

(c) Total pore volume:

The total specific pore volume, V_p, of an adsorbent is generally assumed to be equal to the liquid volume adsorbed at $P/P_0 = 0.98$ of a *Type IV* isotherm shown in Figure 13 above. This evaluation is based on the assumption that the adsorbate has the same molar volume as that of the adsorptive in its normal liquid state at the operational temperature [1]. The total specific pore volume is defined as the liquid volume at a certain predetermined P/P_0, which is a point located after the pore condensation step. The adsorbed amount reflects the adsorbed capacity and the total specific pore volume can be calculated by converting the amount adsorbed into liquid volume. The total pore volume V_p is given by

$$v_p = \frac{w_a}{\rho_l} \tag{6.10}$$

w_a is the adsorbed amount in (grams) and ρ_l is the density of the liquid.

(d) Micropore area and volume:

The *t*-method as proposed by Lippens and de Boer compares an isotherm of a microporous material with a standard *type II* isotherm [97]. The *t*-plot is used to estimate the micropore area and micropore volume of materials. The thickness *t*, of an adsorbed multilayer is calculated from the Harkins and Jura equation, and the external surface area of the sample can be derived from the slope of the *t*-plot. The micropore area is then obtained by subtracting the external surface area from the total surface area earlier obtained from the BET equation. The micropore volume can also be calculated directly from the y-axis intercept of the *t*-plot. The mesopore volume can then be obtained by subtracting the micropore volume from the total pore volume.

All nitrogen sorption measurements in this work were performed with a ASAP 2010 instrument (Micrometrics) at 77 K. The DFT calculations were performed on the Autosorb 1 for Windows 1.25 software (Quantachrome Instruments).

6.6.6. Thermogravimetric analysis (TGA)

Thermogravimetric analysis involves the study of the mass loss of a substance with a controlled temperature programme in a controlled atmosphere as a function of both temperature and time. The programme usually contains a heating or cooling run which is termed dynamic, however there can be isothermal runs in which measurements are made at constant temperature. From TGA measurements, one can determine the amount of molecules contained or adsorbed on samples. The sample is placed in a thermobalance from which the change in mass is obtained. Measurements can be carried out at temperatures as high as 1500 °C and in different gas atmospheres such as helium, nitrogen or oxygen or a mixture of gases.

Modern TGA equipment is usually combined with a mass spectrometer (MS) and/or differential scanning calorimeter (DSC). From the MS and DSC, additional information can be obtained about the desorbed material. For example from the MS, the elements given off during combustion can be determined by the charge-to-mass ratio (m/z) of the element and thus the substance that is adsorbed can be deduced. Also from the DSC the nature of the reaction, i.e. exothermic or endothermic can be determined.

In this work, TGA measurements were performed using a Netzsch TGA 209 and Netzsch STA 449 F1 Jupiter, and the data was analyzed with the Netzsch Proteus Thermal Analysis Software, v. 5.2.1.

6.6.7. Scanning electron microscopy (SEM) and transmission electron microscopy (TEM)

The SEM and TEM techniques are widely used in characterizing the structure and morphology of porous materials. Both techniques are based on electron microscopy wherein an electron beam is used as a source of illumination to form magnified images. An electron microscope is different from a light microscope in that the beam of electrons is used instead of light. The use of electrons therefore gives a huge improvement in resolution because the wavelength of an electron is shorter than that of visible light. The electrons are generated by a tungsten-hairpin gun, and are accelerated through a column towards the sample in the sample chamber. The acceleration is driven by a potential difference (usually 5-20 keV) between the tungsten filament and an anode. A condenser lens is used to condense the beam of electrons and an objective lens is used to focus it to a very fine point on the sample. The beam passes through scanning coils located within the objective lens and the scanning coils deflect the electron beam from side to side in a controlled pattern. The SEM produces images by probing the sample with a focused electron beam that is moved back and forth across the rectangular area of the sample in a controlled sequence known as raster scanning [101, 102]. When the electron beam interacts with the sample, it loses some energy in form of heat, emission of low-energy secondary electrons and high-energy backscattered electrons, light emission or x-ray emission. These different interactions of the electron beam with the sample provide signals and information about the sample surface i.e. its topography and composition. The SEM images are formed by signals with varying intensity coming from the sample and mapped to corresponding positions by the beam. The x-rays emitted from the sample are characteristic of the elements present in the sample. The measurement of these x-rays is called energy dispersive x-ray spectroscopy (EDS). An EDS unit is often attached to a SEM, the detection of the number and energy of the x-rays can be used to make a quantitative analysis of the chemical composition of the sample. SEM images can be up to 100,000 times magnification, with better of depth focus and the images have a three-dimensional appearance which gives realism to surfaces with porous structures [1].

For the TEM on the other hand, the electron beam is accelerated by an anode typically at above 100 keV with respect to the cathode. When taking the image of a sample, the electron beam is condensed and focused by the lenses, and then transmitted through the sample which is in part transparent to electrons and partly scatters them out of the beam. The beam emerging from the sample contains information about the structure which is then magnified by an objective lens. The design and aberration of this lens is of critical importance to the image produced [1, 101]. The final image is obtained by magnifying the intermediate image formed by the objective lens by further lenses situated below the objective and projected onto a fluorescent screen. Magnifications from the TEM can be up to 1,000,000 times the original sample with a point-to-point resolution of about 0.2 nm [1].

SEM images of samples were taken with a Jeol JSM-6335F instrument (Jeol Ltd., Japan) equipped with a Link Inca 300 (Oxford Instruments, UK) EDS unit while TEM images were taken with a JEOL 1400 instrument operated at 200 kV.

7. RESULTS AND DISCUSSION

7.1. Nanocasting

The nanocasting technique was used to prepare a variety of metal oxides such as Fe_2O_3, Co_3O_4, Cr_2O_3, In_2O_3, ZrO_2, NiO, TiO_2, SnO_2 and Mn_2O_3. As stated in the experimental section, different silica templates were used depending on the textural and morphological properties desired in the replica metal oxide. The SEM images in Figure 18 show some of the metal oxides replicated from Daisogel (SP-120-10P and SP-300-10P) used for phosphopeptide enrichment in Paper IV. Metal oxides with other morphologies, for example irregular-shaped morphology (Figure 21), were also synthesized.

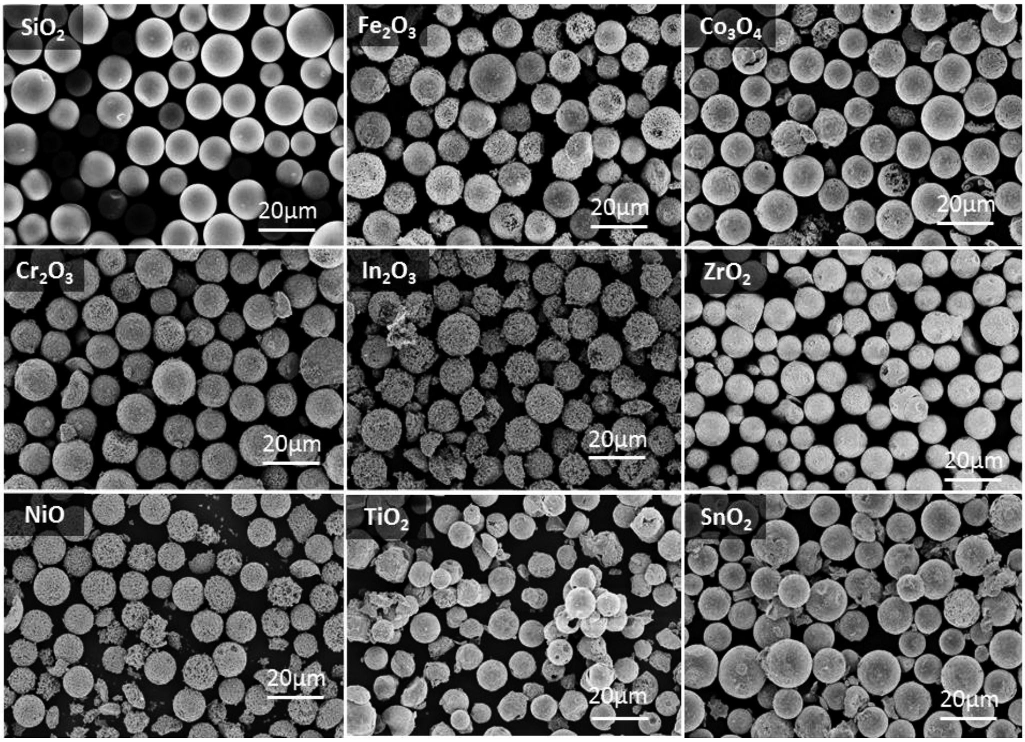

Figure 18: SEM images of some replicated metal oxides and the silica template.

From the SEM images in Figure 18, it is clear that the morphology and size of the nanocast metal oxides are similar to that of the starting silica templates. The similarity indicates that the nanocast metal oxides were successfully replicated. A few broken particles or "fines" can also be seen in failed experiments (shown in Figure 19). Broken particles or fines indicate failed replication (in the sense of the morphology) which may be due to improper impregnation, wrong choice of impregnation method, inadequate number of impregnation cycles, low pore filling degree or deposition of materials outside the pores. Inadequate impregnation cycles or pore filling may lead to the deposition of the precursor outside the pore structure. Further details on the nanocasting process are discussed in the following section. Choosing the right impregnation method is therefore the first step in making successful replicas.

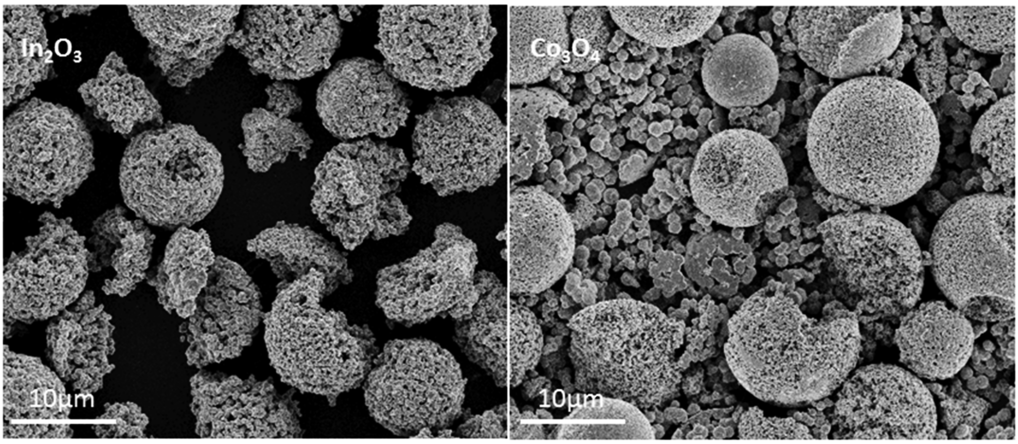

Figure 19: SEM images of some failed nanocasting experiments due to incomplete pore filling

Nitrogen sorption was used to further characterize the metal oxides as shown in Table 1.

Table 1: Nitrogen sorption characterization of the nanocast metal oxides and the EDS results

Metal Oxide	Silica Template Size (nm)	BET Surface Area (m^2/g)	Pore Volume[a] (cm^3/g)	Pore Diameter[b] (nm)	EDS (Si/M) %
TiO_2	30	71.8	0.39	21.8	2.8
SnO_2	12	45.0	0.10	9.0	2.4
ZrO_2	30	66.1	0.29	17.2	5.4
NiO	12	58.8	0.14	9.7	3.9
In_2O_3	12	55.2	0.11	7.5	3.9
Co_3O_4	12	52.1	0.10	7.8	1.3
Fe_2O_3	12	60.9	0.13	8.6	1.4
Cr_2O_3	12	57.5	0.16	11	1.1

[a] Value taken at $P/P_0 = 0.98$

[b] Peak values estimated from the BJH desorption plots

The surface area values show that all the metal oxide spheres are within a range of 42-75 m^2/g which was aimed for in the phosphopeptide enrichment experiments in Paper IV. The pore volumes and diameter are also comparable, and from the EDS, the chemical composition shows that most of the starting silica has been etched away. The higher values for TiO_2 and ZrO_2 are as expected because these metal oxides have strong wetting or interaction with silica, hence being more difficult to remove [25]. The XRD results shown in Figure 20 confirmed the crystal structure of the synthesized metal oxides. The diffraction pattern of the SnO_2 replica displays the typical cassiterite crystal structure (JCPDS card number: 01-070-6995), while the TiO_2 sample fits well to the anatase structure (JCPDS card number: 03-065-5714). The ZrO_2 sample consists mainly of the tetragonal phase (JCPDS card number: 01-072-7115), but traces of monoclinic ZrO_2 can also be detected (JCPDS card number: 00-037-1484). The Fe_2O_3, In_2O_3, Co_3O_4 and NiO samples can be indexed to the JCPDS card numbers: 00-033-0664, 00-006-0416, 01-073-1701, and 00-047-1049, respectively.

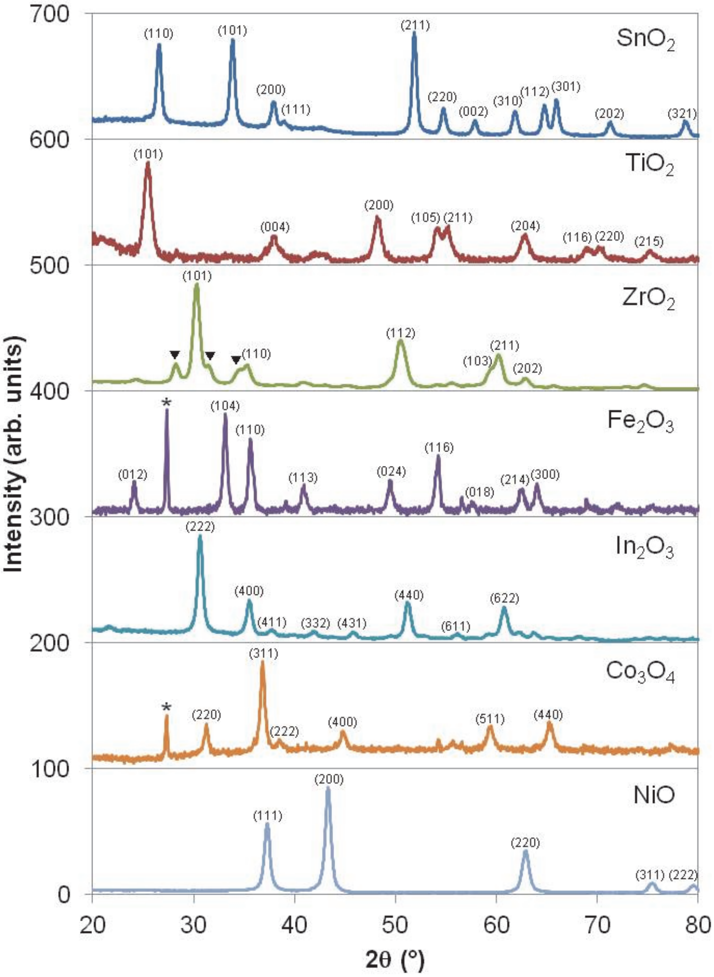

Figure 20: XRD patterns of the different nanocast metal oxide materials. The inverted triangle (▼) indicates trace amounts of monoclinic ZrO_2, while asterisks (*) indicate reflections from the sample holder.

7.1.1. Pore size and textural properties

The porosity of the replicas can be controlled by choosing the templates with desired textural characteristics as shown above. SP-120-10P (silica template with pore width 12 nm and particle size 10 nm) was used as the starting template for all the metal oxides except ZrO_2 and TiO_2 for which SP-300-10P (pore width 300 nm and particle size 10 nm) was used. The templates with larger pores were chosen for ZrO_2 and TiO_2 because higher surface areas were expected due to their strong binding to silica resulting from good wetting of the silica template by the titanium and zirconium ions. Irregular-shaped metal oxides were also replicated from irregular-shaped starting silica used in Paper II as shown in SEM image in Figure 21. The shape and size distribution of the metal oxides are crucial in applications such as chromatography (Paper III) and phosphopeptide enrichment (Paper IV), where spherical particles with narrow size distribution were required for the column packing and for efficient particle collection respectively.

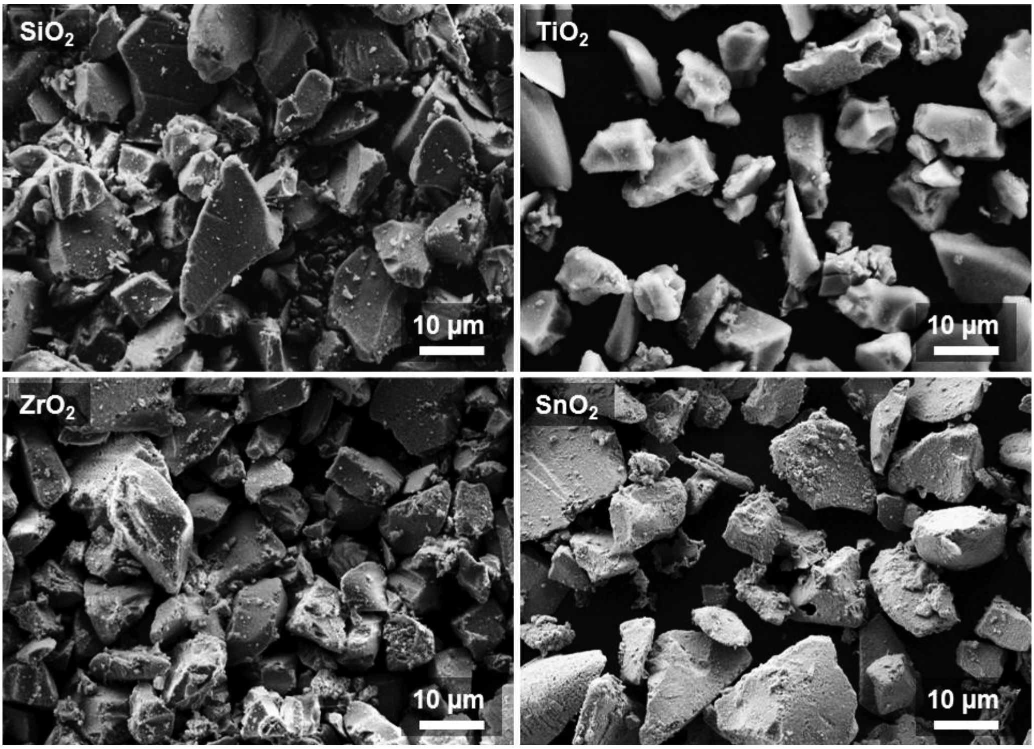

Figure 21: SEM images of nanocast metal oxides from irregular-shaped silica.

7.1.2. Processing conditions

The evaporation or wet impregnation method was the preferred method of infiltration and was mostly used because only 2-3 cycles are required. However, some of the inherent drawbacks of the method include low pore filling degree and deposition of materials outside the pores. These drawbacks cause formation of fines and broken particles. Too many fines or broken particles may block the flow in chromatography or clog capillaries. Therefore, for applications such as capillary electrochromatography and phosphopeptide enrichment (Paper IV) wholesome particles with minimal fines are required. The double solvent method was then used for the nanocasting synthesis of metal oxides used for such applications. Using the double solvent minimized the amount of fines and broken particles because the hydrophobic liquid confines the precursor solution within the pores thus avoiding deposition of materials outside the pores. After the impregnation step, the silica template is dried at a temperature high enough to remove the solvent from the precursor solution. The heating is gradual, as fast heating can lead to quick evaporation of the solvent subsequently leading to loss of some material. This is particularly important if the particles are small (i.e. ≤ 5 µm). After drying, the samples are calcined over a heating ramp up to 550 °C. At this processing temperature the corresponding stable metal oxide crystals are formed from the precursor salt [62, 103, 104]. It is also possible to control the surface area by heating to higher temperatures. For example, TiO_2 sample used in Paper IV was heated to 650 °C after the silica template had been removed in order to reduce the surface area.

7.1.3. Precursor decomposition and formation of the oxide

In order to study the nanocasting technique, SBA-15 silica template was impregnated with nickel (II) nitrate hexahydrate and the heating profile was studied both *in situ* and *ex situ* in Paper I. The hydrated nickel salt has three pairs of water molecules hence the name hexahydrate. During the impregnation and drying process the salt moved into the pores as can be seen from the TEM images in Figure 22 b) where there are darker patches as compared with Figure 22 a) where the pristine SBA-15 silica template is empty. This shows that the pores are homogeneously filled after drying. For the study conducted in Paper I, the pores were intentionally overfilled with the precursor solvent in order to adequately monitor the movement of the salt during the subsequent processing stages. Therefore, the salt is present both inside and outside the pores. Two different gas atmospheres namely helium and air were then used for the calcination process in the study. These two gas atmospheres were chosen in order to compare the effect of different atmospheres on the products of the nanocasting process.

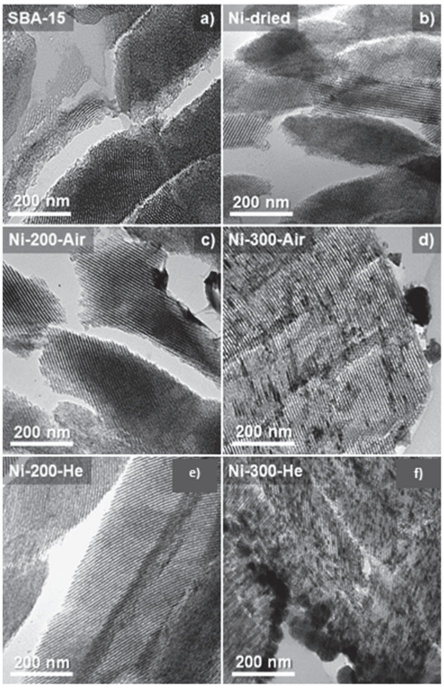

Figure 22: TEM images of the pristine silica (a), the dried sample (b), and the impregnated silica samples heated at 200 °C and 300 °C in He and air respectively(c)-(f).

The transformation from the salt to the oxide is accompanied by the loss of the water of hydration and the decomposition of the salt as the heating temperature increased. Three main steps were identified in the TGA/DSC results shown in Figure 23. Release of hydrate water pairs was observed at ~ 70 °C, 140 °C and then the decomposition into NiO between 210 and 290 °C. The first pair hydrate water was released during the vacuum drying stage.

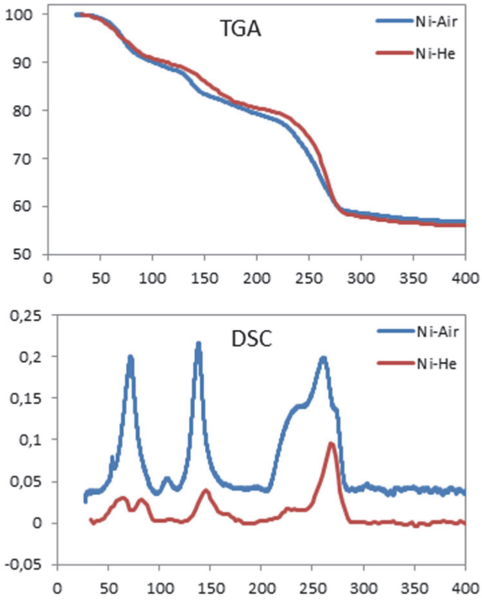

Figure 23: TGA and DSC plots for the Ni-Air and Ni-He samples.

The *in situ* synchrotron XRD measurements showed six distinct sets of diffraction patterns. The diffraction patterns which were similar for either gas atmosphere can be indexed as $Ni(NO_3)_2\cdot 6H_2O$ below ~25 °C, $Ni(NO_3)_2\cdot 4H_2O$ in the range 25–60 °C, $Ni(NO_3)_2\cdot 2H_2O$ in the range 40–150 °C, $Ni(NO_3)_2$ in the range 130–265 °C and nickel hydroxynitrate ($Ni_3(NO_3)_2(OH)_4$) in the range 130–265 °C while a broad NiO reflection begins to show at a temperature of ~220 °C as shown in Figure 24. These patterns show the route or path taken as the salt turns into the oxide.

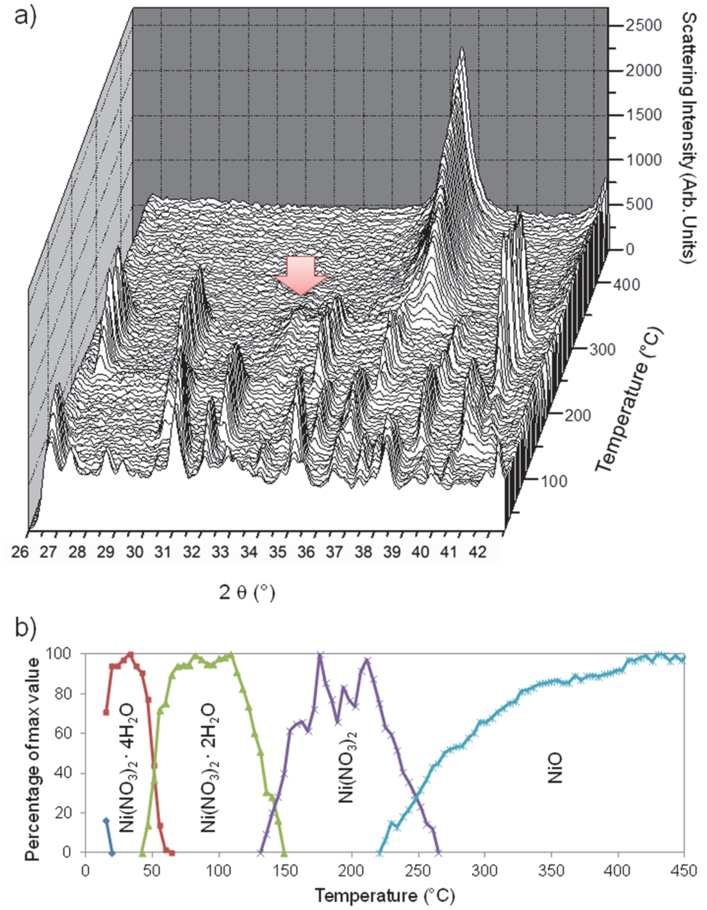

Figure 24: XRD and phase distribution plots as a function of temperature for the Ni-dried sample after heating under air atmosphere. The reflection from the $Ni_3(NO_3)_2(OH)_4$ phase is indicated by an arrow.

The transformation of the salt into the oxide can also be seen from the analysis of the extracted *in situ* SAXS data (Figure 25) which was supported by nitrogen sorption measurements and TEM (see supporting information in Paper I for full details). The changes in d-spacing (i.e. the distance between adjacent lattice planes), the background scattering, the XRD intensity and the electron density are used in explaining the transformation going on as the salt is converted to the oxide.

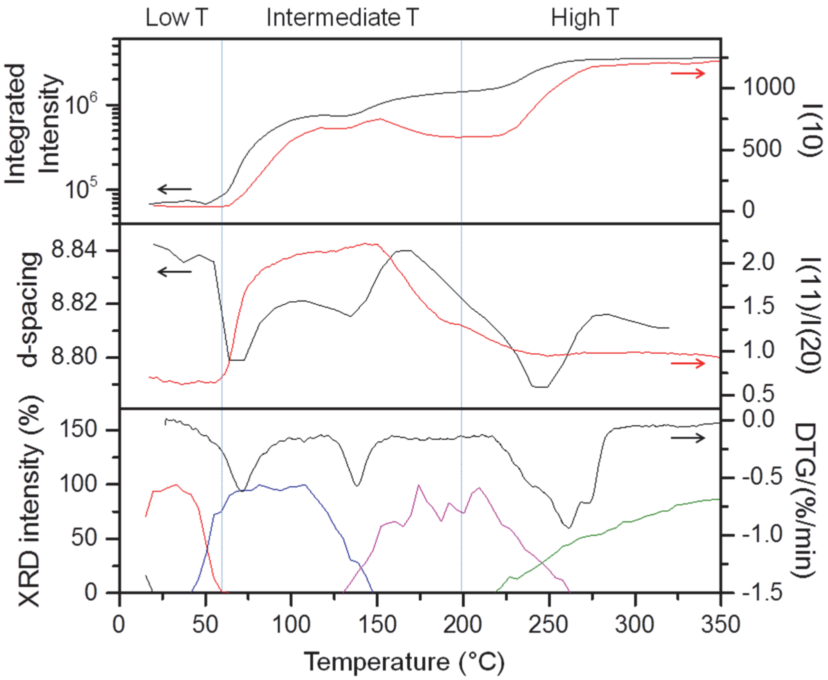

Figure 25: Extracted data from the *in situ* SAXS measurements as a function of temperature ***Top panes:*** Total Integrated intensity under air flow (black line) and under He flow (red line). ***Middle panes:*** The (10) peak position (d-spacing, black line) and the I(11)/I(20) ratio (red line) under air flow only. ***Bottom panes:*** DTG (black line) and XRD phases included for clarity.

At low temperatures (~20-60 °C), a low integrated intensity of the I(10) reflection can be observed (Figure 25). The estimated values for the electron density of the nickel hydrate salts are 0.63 $e^-/Å^3$ for $Ni(NO_3)_2{\cdot}6H_2O$ and 0.68 $e^-/Å^3$ for $Ni(NO_3)_2{\cdot}4H_2O$ which is comparable to 0.66 $e^-/Å^3$ obtained for the silica host. These values show that the electron density contrast between the pore walls and the pores are similar which implies that the mesopores were initially filled as confirmed by nitrogen sorption and the TEM images earlier. As the temperature rises above 60 °C, there is an increase in the integrated scattering of the (10) reflection, as well as increase in the I(11)/I(20) ratio but a decrease in the d-spacing. Changes in the I(11)/I(20) ratio correspond to changes in the relative thickness of the mesopore wall and the mesopore, i.e. when the mesopore size changes with respect to the size of the mesopore walls, the outcome can be seen by changes in the I(11)/I(20) ratio. Such changes can be a result of changes in the electron density due to the presence of salt inside the silica framework (i.e. the porous corona structure). When these intrawall pores are filled with the hydrate salt ($Ni(NO_3)_2{\cdot}6H_2O$ or $Ni(NO_3)_2{\cdot}4H_2O$), the pore radius will appear smaller as the electron density of the salts is similar to that of the silica framework. However, the electron density changes as the dehydrated salt moves into the pores causing an increase in the contrast between the mesopores and the pore walls leading to an apparent increase in the pore radius. The movement of the salt inside or outside the pores is aided by the dehydrated state of the salt. The increase in I(11)/I(20) ratio and decrease in d-spacing signifies the melting of the salt and a contraction of the porous framework as the more electron dense $Ni(NO_3)_2{\cdot}2H_2O$ is formed. The intensity of the (10) reflections continues to increase until a maximum is reached after which it begins to decrease. The decrease of intensity implies that the remaining molten salt outside the pores has solidified and movement into the pores has stopped. After further water evaporation, the electron density reduces hence the decrease in the I(10) reflection. In the temperature range of 180-230 °C, there is a formation of an intermediate nickel hydroxynitrate phase with low mobility as the XRD and TGA/DSC data as well as a strong contraction in the d-spacing suggest.

At 300 °C, distinct NiO nanoparticles can be seen in the TEM images (Figure 22). The intensity of the (10) reflection begins to rise again (at temperature > 230 °C) as the electron dense and crystalline NiO phase is formed. From the nitrogen sorption data (see Paper I), there is a broadening of the hysteresis loop for the samples at 300 °C, due to the formation of NiO particles and reorganization of the particles into aggregates at different spots. These aggregates and empty pores can also be seen from the TEM images. The delayed desorption effect seen in the nitrogen sorption suggests partially blocked pore opening which may be due to some NiO aggregates in the pores. Further increase in temperature up to 500 °C shows an increase in XRD intensity of the NiO phase as a result of the growth and sintering of the oxide. The etched oxides showed no mesoscopic order as the morphology of the original SBA-15 was not retained. The fidelity of replication could not be retained due to the low mesopore filling by the NiO and low intrawall pore filling at high temperatures.

There were slight differences observed in the formation stages described above for the different gas atmospheres. For example, the mass loss due to the evaporation of hydrate water in helium gas atmosphere occurred over a wider temperature range when compared to air atmosphere. However, in general terms, the formation route and stages were similar for both gas atmospheres although larger NiO aggregates could be seen in the helium samples due to higher mobility of nickel compound in helium atmosphere. More details about the differences in the atmospheres can be seen in Paper I. These results show the transition of a metal nitrate salt to the oxide and may be applicable to all metal nitrates in general as a similar trend was seen for cobalt nitrate in a similar study.

In summary, the oxide is formed as the water of evaporation is lost through the formation of the intermediate nickel hydroxynitrate and then the oxide. After the oxide is formed, it clusters or clumps together at suitable spots along the pores. Therefore, in order to form wholesome particles which have a true replication of the morphology of the starting template the following points are crucial:

- The pores of the template must be adequately filled with little or no precursor deposited outside the pores. The double solvent method of infiltration was particularly excellent in this regard as hydrophobic solvent ensures that the precursor solution is ‘locked’ inside the pores. The broken spheres seen in Figure 19 were due to inadequately filled pores. The experiments were repeated with adequate pore filling and wholesome particles were produced (Figure 18).

- During the nanocasting process, the salt moves to nucleation sites which are the suitable spots on the pore walls where the salt-oxide (transition form of the oxide) nucleates. From these nuclei, it grows into aggregates while filling the pores. This is perhaps the most crucial stage as the pores must be adequately filled by the salt-oxide in order to obtain true replication of the morphology of the template material.
- Using the He gas flow hinders the formation of the intermediate phase (nickel hydroxynitrate) and subsequently the oxide becomes more mobile which leads to better pore filling and replication.

7.2. Surface modification

7.2.1. Degree of modification

The metal oxides in Paper II (SnO_2, TiO_2 and ZrO_2) nanocast from irregular-shaped silica templates (Figure 21) and in Paper III (Mn_2O_3, SnO_2, and ZrO_2) from spherical spheres were functionalized with amino groups using different strategies. The modification techniques were covalent bonding of 3-aminopropyltriethoxysilane (APTES), chemisorption of 2-aminoethyl dihydrogen phosphate (AEDP), electrostatic interaction with polyethyleneimine (PEI), and surface polymerization with aziridine (AZ). Nitrogen sorption results for the unmodified metal oxides and modified metal oxides in Table 2 show that they remained porous after functionalization. However, the table also contains the changes in the textural properties such as the BET surface area, pore volume and *c* value which suggest that the surface of the metal oxides have been modified. The *c* values extracted from BET plots are of particular importance because they depict the interaction of the nitrogen molecules with the sample. If the *c* value is high, it means there is a strong interaction of the nitrogen molecules with the adsorbate as a result of hydrophilic groups on the surface or a microporous surface structure. However, if the *c* value is low the interaction of the nitrogen molecules is weak due to the presence of organic molecules on the surface as the surface becomes more hydrophobic.

Thermogravimetric analysis (TGA) and the ninhydrin spectrophotometry method were used to quantify the amount of amino groups attached to the surface of the metal oxides while electrokinetic measurements as a function of pH were used to obtain isoelectric points (IEP) of the nanocast metal oxides.

Table 2: Results of modification/functionalization of some nanocast metal oxide.

Sample	**BET Surface Area (m^2/g)**	**Pore Volume[a] (cm^3/g)**	**Pore Size[b] (nm)**	***c* Value**	**Γ_{TGA} ($\mu mol/m^2$)**	**$\Gamma_{ninhydrin}$ ($\mu mol/m^2$)**	**IEP**
SiO_2	454	0.73	5.8 (4.8)	81	-	-	3.5
SiO_2-APTES	346	0.50	4.9 (4.3)	42	3.0	10.4	8.3
SiO_2-AEDP	418	0.68	5.7 (4.8)	71	0.8	< 0.5[c]	3.5
SiO_2-AZ	248	0.41	4.9 (4.4)	32	9.8	15.3	10.3
SiO_2-PEI	339	0.62	5.7 (5.0)	34	7.3	8.9	10.2
TiO_2	237	0.60	12.4 (8.9)	51	-	-	5.0
TiO_2-APTES	173	0.44	10.8 (8.9)	36	2.9	2.4	8.9
TiO_2-AEDP	224	0.58	12.5 (9.1)	51	5.2	1.6	~3.8[d]
TiO_2-AZ	167	0.51	11.7 (10.2)	34	10.6	24.9	10.5
TiO_2-PEI	186	0.51	12.2 (9.5)	35	12.5	15.6	10.9
ZrO_2	189	0.47	6.3; 20.4 (8.1)	64	-	-	5.0
ZrO_2-APTES	141	0.35	5.6; 16.5 (8.1)	36	6.5	2.8	9.9
ZrO_2-AEDP	159	0.42	6.2; 19.9 (8.2)	54	2.9	< 1.2[a]	4.0
ZrO_2-AZ	137	0.35	5.6; 18.6 (8.3)	33	11.1	5.0	9.5
ZrO_2-PEI	149	0.39	5.9; 19.5 (8.8)	30	9.9	1.8	10.3
SnO_2	59	0.135	4.4 (6.6)	65	-	-	3.4
SnO_2-APTES	55	0.119	3.8 (6.6)	38	2.5	14.2	9.2
SnO_2-AEDP	58	0.128	4.3 (6.6)	56	2.1	< 2.0[a]	4.5
SnO_2-AZ	55	0.121	4.1 (6.4)	37	6.1	9.5	6.3
SnO_2-PEI	56	0.118	3.8 (6.3)	33	9.4	4.3	9.4

[a] Value taken at $P/P_0 = 0.98$.

[b] Peak values estimated from the BJH desorption plots (in brackets are the mean BJH pore size values).

[c] The values are below the detection limit of the ninhydrin adsorption method.

[d] The zeta potential value for this sample was very close to 0 mV in the pH range 2.4–5.1.

The TGA results in Table 2 show the amount of organic groups attached to the surface while the ninhydrin spectrophotometry result show the amount of reactive accessible amino groups. The success of modification was also qualitatively assessed by FTIR (see Paper II for more details).

The *c* values of all the modified metal oxides reduced significantly. APTES, AZ and PEI modifications gave lower values compared to AEDP which gave values very close to the unmodified metal oxides. TGA were then used to gain further insight about the packing density. The estimated surface coverage showed that the monomeric compounds APTES and AEDP had surface excess value of 2-3 $\mu mol/m^2$ while the polymeric compounds had

~10 μmol/m^2. The reactivity of the accessible amino groups was also determined by the ninhydrin spectrophotometric method. The result shows that APTES-, AZ- and PEI-modified samples all have high surface excess values of reactive amino groups with values between 2 and 25 μmol/m^2. For AEDP-modified samples, the amount of accessible amino groups was typically below the detection limits. Finally, to confirm that the modification by the different methods has augmented the surface chemistry, the IEP of the modified metal oxides was measured and compared with the unmodified metal oxides. It can be seen from the IEP results that there is a shift in the values for modified metal oxides which indicate a successful modification. APTES, AZ and PEI had large shifts of the IEP while AEDP did not have any significant shift. This suggests that the AEDP modification was not an efficient modification most likely because of the large phosphate anchoring group which may have cancelled out the positive charge of the amino group. APTES, AZ and PEI on the other hand could be used to synthesize highly functional metal oxide surfaces.

7.2.2. Stability tests

The hydrolytic stability of the modification on the surface of the metal oxide was also tested by zeta potential measurements in acidic conditions (pH 2) and in basic conditions (pH 10) after different chosen time intervals. These pH values are of particular interest in separation processes. An example of the results of the stability test for ZrO_2 is shown in Figure 26. The zeta potential measurements were used to verify how much of the amino groups was retained on the metal oxide surface after aging in acidic and basic conditions over a certain period of time. Full results for the other metal oxides can be found in Paper II.

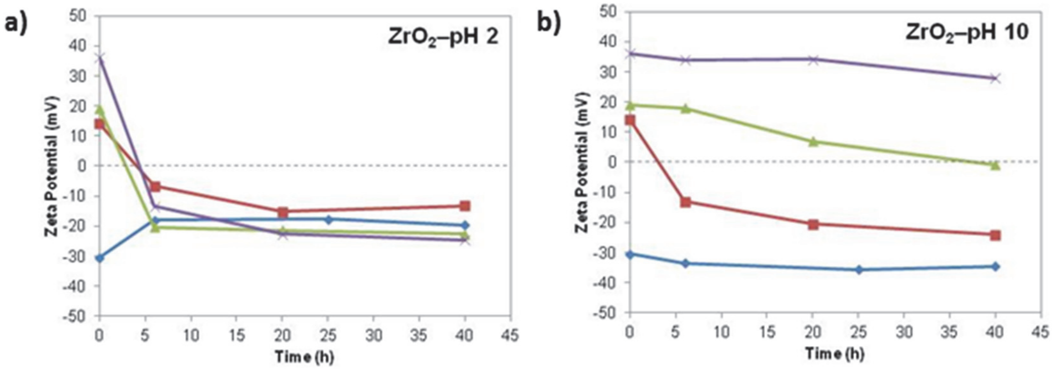

Figure 26: Hydrolytic stability chemical modifications (measured as zeta potential at pH 7.2 in HEPES buffer) after treatment at pH 2 for certain amounts of time, where ◆ indicates ZrO_2, ■ = ZrO_2-APTES, ▲ = ZrO_2-AZ, and × = ZrO_2-PEI, respectively.

A decrease in the zeta potential values after a certain time at pH 2 or 10 would indicate that the amino groups have hydrolytically been removed from the surface. From the results, the PEI modified samples were the most stable at pH 10.

In summary, metal oxides were successfully prepared with the nanocasting technique after which the surface of these metal oxide particles were modified with amine compounds namely APTES, AEDP, PEI and AZ using four different approaches. The degree of modification were verified with thermogravimetry, ninhydrin spectrophotometry and zeta potential titrations. The hydrolytic stability of these amine groups on the surface of the oxides were also examined by aging at pH 2 and 10 for a certain period of time.

- Surface excess values estimated from TGA and ninhydrin spectrophotometry and a large shift of the IEP indicate that the surface modification was successful with all the amine functional groups except for AEDP.
- AEDP was unable to create an efficient modification probably because of its large phosphate anchoring group which might cancel out the positive charge of the amino group.
- SiO_2-AZ, ZrO_2-AZ, SiO_2-PEI, ZrO_2-PEI and SnO_2-PEI had exceptional hydrolytic stability at pH 10 as there was only a marginal decrease in the zeta potential values after aging for 40 h. On the other hand, all the APTES-, AZ- and PEI-modified metal oxide samples were fairly stable at pH 10 after aging for a similar period of time while only SnO_2-APTES and SnO_2-PEI could be considered fairly stable after aging at pH 2.

7.3. Chromatography

In Paper III, APTES-functionalized SiO_2 microspheres and aziridine (AZ)-functionalized metal oxide microspheres SnO_2, Mn_2O_3, ZrO_2 (prepared by nanocasting) and SiO_2, were used as packing materials for capillary electrochromatography (CEC) and capillary liquid chromatography (CLC) columns. The purpose of these functionalizations was to enable both electrostatic and hydrophobic interactions with the selective compounds and thus separating them. SiO_2-APTES and SiO_2-AZ were comparatively easily packed into CLC columns reaching about a length of 23 cm in 1 h. However, the AZ-functionalized SnO_2, Mn_2O_3 and ZrO_2 packed under the same conditions caused blockages such that only 3 or 4 cm could be packed. It was observed through the microscope that the positively charged AZ-functionalized metal oxides adsorbed onto the negatively charged capillary leading to an eventual blockage of the capillary. Capillary coatings made with APTES and polyacrylamide were then used to solve the problem. APTES has positively charged amino groups while polyacrylamide is neutrally charged, hence no attraction to the capillary columns takes place. The coating with APTES and polyacrylamide improved the column-packing as ZrO_2-AZ was successfully packed into the column and a column length of 10 cm was packed with SnO_2-AZ. Packing with Mn_2O_3-AZ was also done but only after pre-conditioning with a pH 2 solution.

For CEC packing, SiO_2-AZ particles were packed using the electrokinetic method after a pre-conditioning with pH 2 solution which is to prevent the dissociation of the silanol groups on the silica capillary surface. However, a packing length of only 3 cm was achieved. The other metal oxides could not be packed because they are slightly electrically conductive (especially SnO_2 and Mn_2O_3) and as such could not be used because of bubbles formation due to redox reactions. SiO_2 was therefore used in the subsequent chromatography tests. Functionalized-SiO_2-packed CEC column was used for separation of acidic and neutral compounds, for example a mixture of four isomers of dihydrobenzoic acid and two organic acids (see details in Paper III).

Furthermore, separation of some neutral compounds was carried out to study the hydrophobicity of SiO_2-AZ. A mixture of acetone, phenol and benzene were separated with SiO_2-Az-packed-columns which showed that the materials are hydrophobic (see Figure 27a). Likewise SiO_2-APTES also gave electrostatic and hydrophobic interactions as shown in Figure 27b.

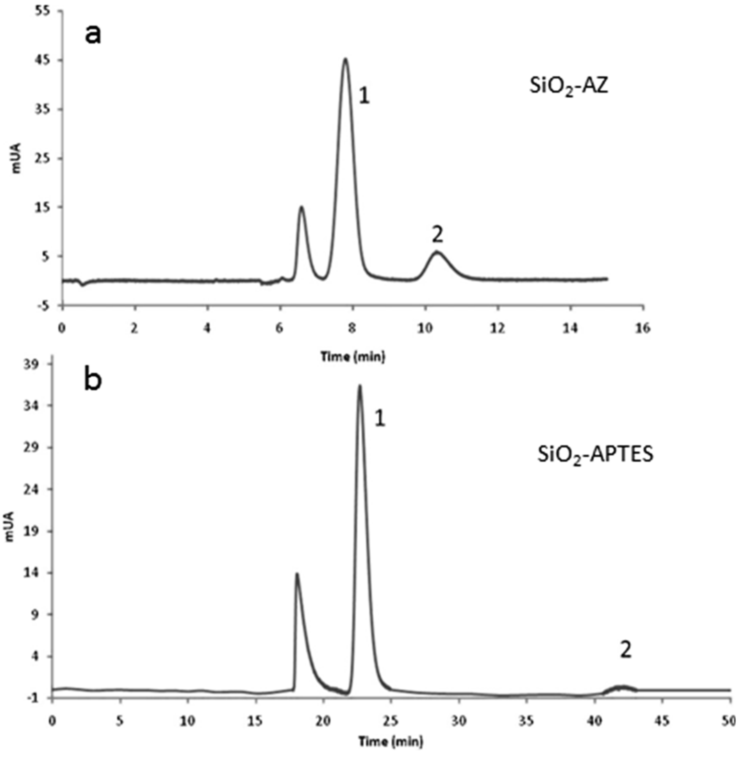

Figure 27: CEC separation of (1) phenol and (2) benzene by columns packed with (a) SiO_2-AZ and (b) SiO_2-APTES.

The AZ-functionalized Mn_2O_3 could not be packed into CEC columns due to instable current and the formation of bubbles. However, it was used as stationary phase in CLC. However, for the separation of substituted benzoic acid the Mn_2O_3-AZ was not successful either as the analytes co-eluted at 4 min as shown in Figure 28 (A). SnO_2-AZ packed capillaries were also tested in the separation but only three peaks were obtained in the chromatogram as shown in Figure 28 (B).

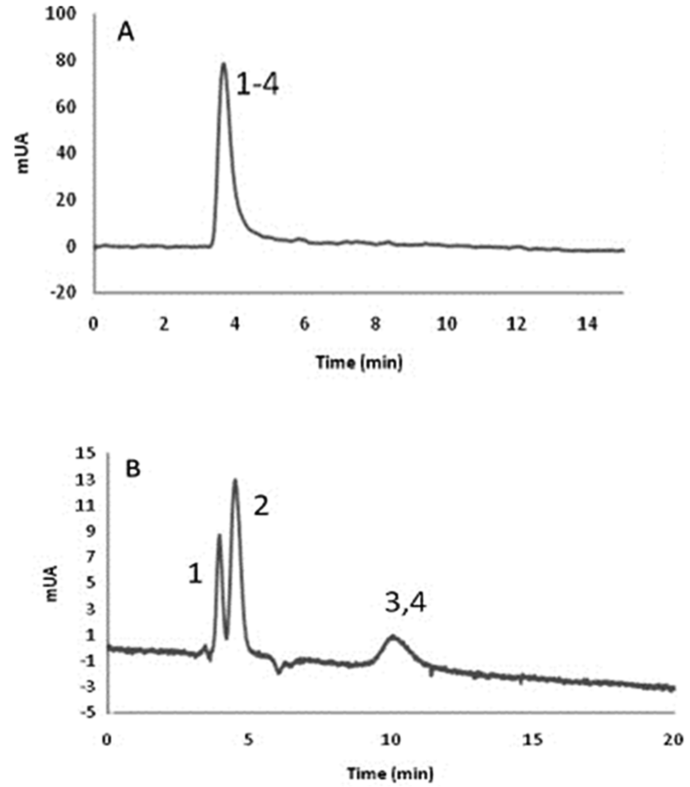

Figure 28: CLC separation of substituted benzoic acids with capillaries packed with: (A) AZ-functionalized Mn_2O_3 (B)AZ-functionalized SnO_2. Analytes are: (1) 2,6-dihydroxybenzoic acid;(2) 2,5-dihydroxybenzoic acid;(3) 2,4-dihydroxybenzoic acid; (4) 3,5-dihydroxybenzoic acid.

In summary, SnO_2, Mn_2O_3, ZrO_2 (prepared by nanocasting) and SiO_2 were functionalized with aziridine and APTES (SiO_2 only) for application as capillary packing in CEC and CLC. The AZ-functionalization was to give both electrostatic and hydrophobic interactions with selective compounds.

- The TGA, zeta potential and nitrogen sorption measurements were used to confirm the success of the functionalization. The modified metal oxides were also found to be hydrolytically stable. The modification of the metal oxides enabled them to be used in LC applications without altering the desirable morphological properties as porous materials.
- SiO_2-APTES and SiO_2-AZ could be packed into capillaries of 23 cm in length while the other functionalized metal oxides could only be packed for 3 or 4 cm because of blockages which were as a result of interactions between the charged surface of

the modified metal oxides and the capillaries. The blocking was however resolved by coating the capillaries with APTES and polyacrylamide (PAA) after which only ZrO_2-AZ was successfully packed at pH 2. SnO_2 and Mn_2O_3 could not be packed because of their slight electrical conductivity.

7.4. Phosphopeptide enrichment

The nanocast metal oxides were also used in phosphopeptide enrichment tests. Nine different metal oxides (SnO_2, TiO_2, ZrO_2, Fe_2O_3, In_2O_3, Co_3O_4, NiO, Mn_2O_3 and Cr_2O_3) were tested in a performance screening exercise after which seven were used for tests with synthetic peptides and later some actual biological samples. The nanocasting technique enabled the synthesis of metal oxides with comparable morphological properties and BET surface areas within a certain range (42-75 m^2/g). Having the nanocast materials within a certain range eliminates differences in surface area which is one major source of variability, as widely varying properties of MOAC sorbents have made comparison of the performance difficult in the past.

The first step was to screen the metal oxides based on their relative binding affinities to synthetic phosphopeptides. Nine synthetic phosphopeptides including one diphosphopeptide were used in the screening, with nine different nanocast metal oxides and two commercial TiO_2 (Titansphere and Sachtopore). The binding strength of the metal oxide to the phosphopeptide was used to rank the performance of the metal oxides. The binding in the presence or absence of lactic acid (LA) which is a competitor for phosphate binding sites was also used in the ranking. Addition of LA reduces the non-specific binding of acidic unphosphorylated peptides which therefore improves the specificity of the enrichment procedure [105]. Figure 29 (a) shows the ranking of the metal oxide. Cr_2O_3 and Mn_2O_3 were not ranked as their phosphate affinity was considered too low to be quantified by the liquid chromatography-tandem mass spectrometry (LC-MS/MS) used for identification and label-free quantification of the peptides.

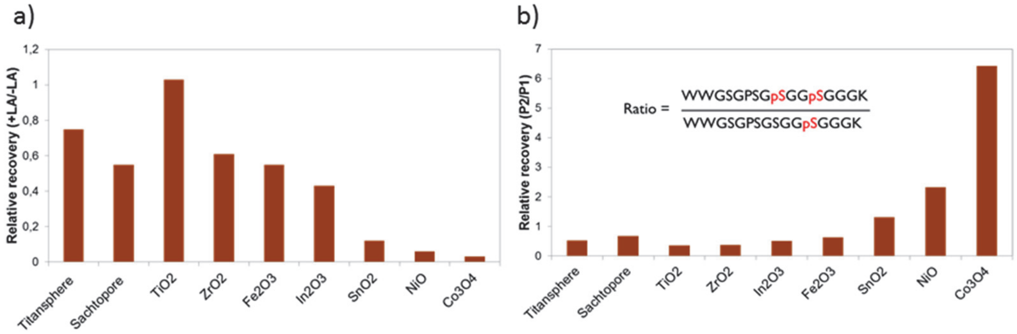

Figure 29: (**a**) Phosphopeptide affinity screening of nanocast metal oxides (**b**) The relative recoveries of singly (1P) and doubly (2P) phosphorylated peptides in the presence of lactic acid for the different materials.

The phosphate binding in the presence or absence of lactic acid reflects the phosphate affinity of the metal oxides. It can be seen that the phosphate affinity of nanocast TiO_2 was better than for the commercial TiO_2 materials Titansphere and Sachtopore while ZrO_2 was comparable to them. Fe_2O_3 and In_2O_3 also showed comparable binding strength; the case of In_2O_3 is quite interesting as this is the first time it is being used as an enrichment material and it showed good prospects. In Figure 29 (b) however, the weaker binding metal oxides showed higher specificity in binding the doubly (2P) phosphorylated peptides. These metal oxides (e.g. NiO and SnO_2) show high intrinsic specificity and can therefore serve as complementary affinity sorbents.

After the first screening exercise, the binding strength of the nanocast metal oxides was evaluated using more complex samples e.g. cell lysate samples. This was done in order to show that the peptide identification by the nanocast materials can be applied to actual biological samples. Seven nanocast metal oxides and Titansphere were thus selected for the enrichment tests with protein digests of lysates from the human embryonic kidney cell line, HEK293. Figure 30 shows a comprehensive summary of the results for all materials evaluated. ZrO_2 gave most identifications (3758) while In_2O_3 also performed creditably well with 3626 identifications. The number of phosphopeptides identified by In_2O_3 is comparable to 3648 identified by Titansphere which is the standard. The peptide identifications by Co_3O_4, NiO and SnO_2 were however smaller due to the weaker affinity of these materials as shown in the previous exercise. However, these weaker affinity oxides namely NiO and Co_3O_4 are able to identify higher percentage of the multiply-phosphorylated peptides.

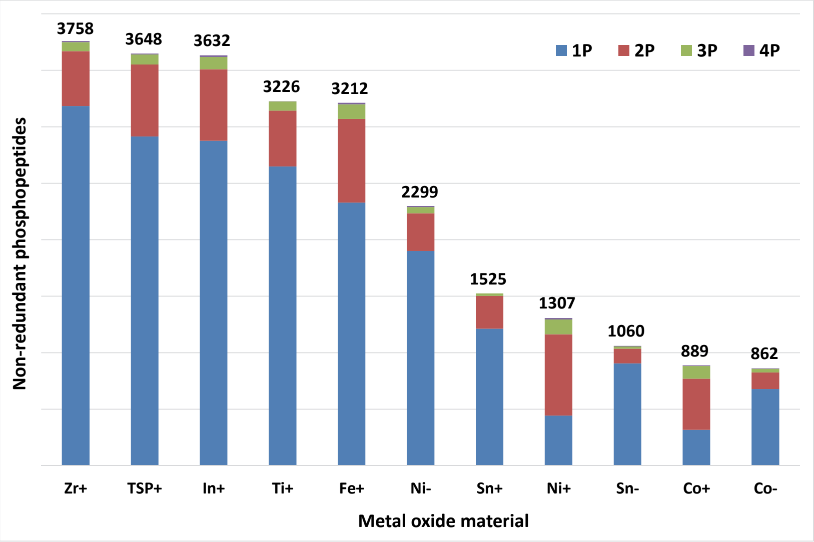

Figure 30: Non-redundant phosphopeptides with confident site localization identified with the different metal oxides affinity materials.

In order to explain the performance observed, the surface chemistry of the oxides was studied by zeta potential titrations from which the experimental IEPs of the metal oxides were determined. The performance of the metal oxides clearly followed the trend of the IEP as shown in Table 3 (except for SnO_2).The IEP increases in the order SnO2<TiO_2<ZrO_2 ~Fe_2O_3~In_2O_3<Co_3O_4<NiO. For further insight, the metal oxides were ranked according to their acidity values based on the acidity scale (N_M-$2\delta_M$) by Jeong et al [106]. The IEP values are roughly the inverse of the N_M-$2\delta_M$ acidity scale.

Table 3: Surface chemistry and acidity values of the metal oxides.

Metal oxide	Isoelectric points[b]	Acidity values[a] ($N_M-2\delta_M$)	Residual SiO_2[c] (Si/(Si+M) at-%)
SnO_2	3.9	3.47	2.4
TiO_2	5.7	3.05	3.4
ZrO_2	5.6	2.59	5.2
TSP	7.0	3.05	-
Fe_2O_3	8.1	2.49	1.9
In_2O_3	5.9	2.47	4.0
Co_3O_4	8.8	2.63 and 1.51*	1.2
NiO	8.7	1.50	3.2

[a]Values extracted from[106]. [b]Determined from electrophoretic titrations. [c]Determined from EDS measurements. *Co_3O_4 is a spinel structure consisting of Co_2O_3 and CoO, and thus these acidity values have been listed.

The acidity scale is based on the electronegativity of the metal oxides, the symbols N_M and $2\delta_M$ represent the formal oxidation state in a compound and the partial charges in metal oxides respectively. The (N_M-$2\delta_M$) values represent the Lewis acid strength of the oxide being controlled by the interplay of the formal oxidation state (N_M) and the partial charges ($2\delta_M$). The (N_M-$2\delta_M$) value can be readily derived from the stoichiometry and the Sanderson's electronegativity values of the metals [106]. Ranking the metal oxides studied based on the list in Table 3 therefore, SnO_2, ZrO_2 and TiO_2 are the 'most' acidic, Fe_2O_3 and In_2O_3 are 'mildly' acidic while Co_3O_4 and NiO are 'least' acidic. The performance of the metal oxides in the enrichment study correlates to the measured IEP values and supported by the acidity ranking in Table 3. ZrO_2 which is one of the most acidic identified the highest number of peptides. The least acidic metal oxides correspondingly identified the least number of peptides. Interestingly however, the least acidic oxides were able to identify more peptides with multiple phosphorylated sites.

In conclusion on the correlation of the performance and the physicochemical properties of the metal oxides, it is clear that the affinity of the metal oxides can be related to the acidity ranking and the IEP. It should also be pointed out that there are some glaring deviations from this acidity ranking and IEP results. These deviations, for example the performance of Fe_2O_3 and In_2O_3 may be related to the porosity of the metal oxides and the amount of residual silica. The N_M-$2\delta_M$ acidity values were only based on metal oxides, their porosity was not considered. Moreover, the residual silica in the nanocast materials may form hydroxyl groups when in solution which may affect the acidity of the oxides. Surface effects including hydration and redox reactions which may cause shifts in the IEP results may also contribute to these deviations.

In summary, the nanocasting technique has been used to prepare materials with surface areas and pore sizes within a certain range. Thus, allowing a comparative study of different phosphopeptide enrichment materials.

- A screening exercise based on the binding affinity of the metal oxides to synthetic phosphopeptides was first performed to select the seven nanocast metal oxides that were subsequently used in the comparative study. From this screening exercise, the phosphate affinity of nanocast TiO_2 was better than the commercial TiO_2 Titansphere while Fe_2O_3 and In_2O_3 also showed sufficient binding strength. Mn_2O_3 and Cr_2O_3 were eliminated in this screening exercise.

- In the main comparative study, cell lysate which are more complex than synthetic phosphopeptides used in the screening exercise were used. ZrO_2 identified more phosphopeptides than any other material including the commercial ones. The remaining oxides performed creditably as well, NiO and Co_3O_4 which identified the least amount of phosphopeptides were interestingly able to identify more multiply-phosphorylated peptides.

- The physicochemical properties of the nanocast metal oxides were correlated with their performance by using an acidity scale and measured IEPs. The performance of the materials was ranked as $SnO_2 < TiO_2 < ZrO_2 \sim Fe_2O_3 \sim In_2O_3 < Co_3O_4 < NiO$.

- Having a complementary affinity study of different metal oxide materials offers a more complete representation of biological events, especially for highly phosphorylated peptides which may be missed by standard protocols.

8. CONCLUSIONS

This thesis has been able to pinpoint the crucial stages in the nanocasting technique. Using nickel nitrate hexahydrate as an example, the transformation of a metal salt to the oxide has been clearly explained. The procedure used in this study can thus be applied to study other metal oxides. The thesis has also shown how to control these stages such that the morphology of the starting template is successfully replicated. This knowledge can be useful in preparation of materials with true fidelity of replication, and also limit or eliminate defects in nanocast materials using efficient synthesis procedures.

Successful replicas have also been modified with organic moieties and shown to be stable in acidic and basic conditions. The hydrolytic stability of functionalized materials has also been studied. It can be clearly seen that APTES, AZ and PEI could provide highly functionalized metal oxide surfaces. In addition to the functionalized silica materials, PEI and AZ-functionalized SnO_2, ZrO_2 and SiO_2 showed exceptionally good chemical stabilities. These results can be instructive when alternatives to amino-functionalized silica materials are being considered.

Furthermore, nanocast metal oxides (SnO_2, Mn_2O_3 and ZrO_2) and SiO_2 were functionalized with aziridine and APTES in order to have electrostatic and hydrophobic interactions with selective compounds. The functionalized materials were subsequently packed into CEC and CLC columns. However, only SiO_2-APTES and SiO_2-AZ could be packed into the columns, the other materials could not be packed because of blockages. The blockages were found to be a result of interactions between the positively charged particles and the negatively charged capillaries. The AZ-functionalized silica particles showed good stability, hydrophobic and ion exchange interactions over a wide pH range which suggests its suitability as a column packing material in both CLC and CEC.

Finally, the nanocasting technique was used to prepare nanocast materials with surface area and pore sizes in the range of 45-72 m^2/g. Having the materials within this range enabled the comparison of the binding affinities of the different materials. The nanocast metal oxides were able to identify singly and multiply phosphorylated peptides. The performance of nanocast metal oxides was comparable and at times better than the standard which is Titansphere. In_2O_3 was also used in enrichment studies for the first time and found to be very efficient. The performance of the metal oxides was then ranked based on their acidity values and isoelectric points (IEPs). These results give a useful correlation between the physicochemical properties and the performance of the enrichment materials which may be instructive in the selection of materials for specific enrichment procedures.

9. ACKNOWLEDGEMENTS

My sincere and very deep appreciation goes to my supervisor Dr. Jan-Henrik Smått, first for giving me a chance in his project and supporting me through 'thick and thin' in the course of the doctoral process. My gratitude goes as well to Prof. Jouko Peltonen for the overall support and enabling environment provided.

I want to also thank all co-authors especially Prof. Mika Lindén and Dr. Alexander Leitner for fruitful collaborations.

The Academy of Finland and Åbo Akademi Stifstelsen are acknowledged for financial support.

I wish to also thank the Fyke family (past and present) for a friendly and caring atmosphere where ideas thrive. I'll like to specially thank Tina Gulin-Sarfraz for being a nice 'roomie'- sharing cookies and chocolates with me and helping with the inevitable language issues; as well as Christina Luojola for always helping with a smile.

Many thanks to my Pastors, Björn & Laura Bergvall and Olatunde & Daniella Olubode for spiritual support and encouragement as well as the Nigerian community in Turku Finland especially Dr. Ikenna Anugwom for making living in Turku a pleasure.

Most sincere gratitude to my family members especially my lovely wife (*Abeks*) for providing a peaceful atmosphere to enjoy my work.

Lastly, I give all adoration and thanks to God-my refuge & strength for His sustenance.

10. REFERENCES

[1]. Schüth F, Sing KSW, Wietkamp J. Handbook of porous solids. *Wiley-VCH* 2002; **1**.

[2]. Lu A-H, Schüth F. Nanocasting: A versatile strategy for creating nanostructured porous materials. *Adv Mater* 2006; **18**:1793-1805.

[3]. Lu A-H, Zhao D, Wan Y. Nanocasting- A versatile strategy for creating nanostructured porous materials. *RSC Nanoscience & Nanotechnology* 2010.

[4]. Sing KSW. Adsorption methods for the characterization of porous materials. *Adv Colloid Interface Sci* 1998; **76–77**:3-11.

[5]. Ciesla U, Schüth F. Ordered mesoporous materials. *Microporous and Mesoporous Materials* 1999; **27**:131-149.

[6]. Taguchi A, Schüth F. Ordered mesoporous materials in catalysis. *Microporous and Mesoporous materials* 2005; **77**:1-45.

[7]. Neouze M-A, Schubert U. Surface modification and functionalization of metal and metal oxide nanoparticles by organic ligands. *Montash Chem* 2008; **139**:183-195.

[8]. Sturm M, Leitner A, Smått J-H, Lindén M, Lindner W. Tin dioxide microspheres as a promising material for phosphopeptide enrichment prior to liquid chromatography-(tandem) mass spectrometry analysis. *Adv Func Mater* 2008; **18**:2381-2389.

[9]. Williams DE. Semiconducting oxides as gas-sensitive resistors. *Sens Actuators B* 1999; **57**:1-16.

[10]. Smått J-H, Lindén M, Wagner T, Kohl C-, Tiemann M. Micrometer-sized nanoporous tin dioxide spheres for gas sensing. *Sens Actuators B* 2011; **155**:483-488.

[11]. Li Y, Fu Z-Y, Su B-L. Hierarchically structured porous materials for energy conversion and storage. *Adv Funct Mater* 2012; **22**:4634-4667.

[12]. Yang P, Gai S, Lin J. Functionalized mesoporous silica materials for controlled drug delivery. *Chem Soc Rev* 2012; **41**:3679-3698.

[13]. Xing Z-C, Chang Y, Kang I-K. Immobilization of biomolecules on the surface of inorganic nanoparticles for biomedical applications. *Sci Technol Adv Mater* 2010; **11**:1-17.

[14]. Nawrocki J, Dunlap C, McCormick A, Carr PW. Part I. Chromatography using ultra-stable metal oxide-based stationary phases for HPLC. *J Chromatogr A* 2004; **1028**:1-30.

[15]. Nawrocki J, Dunlap C, Li J, Zhao J, McNeff CV, McCormick A, et al. Part II. Chromatography using ultra-stable metal oxide-based stationary phases for HPLC. *J Chromatogr A* 2004; **1028**:31-62.

[16]. Jose R, Thavasi V, Ramakrishna S. Metal oxides for dye-sensitized solar cells. *J Am Ceram Soc* 2009; **92**:289-301.

[17]. Stratakis E, Kymakis E. Nanoparticle-based plasmonic organic photovoltaic devices. *Materials Today* 2013; **16**:133-145.

[18]. Jiang Q, Aya N, Shi FG. Nanotube size-dependent melting of single crystals in carbon nanotubes. *Appl Phys A* 1997; **64**:627-629.

[19]. Sun C, Lee JSH, Zhang M. Magnetic nanoparticles in MR imaging and drug delivery *Advanced Drug Delivery Reviews* 2008; **60**:1252-1265.

[20]. Pan F, Song C, Liu XJ, Yang YC, Zeng F. Ferromagnetism and possible application in spintronics of transition-metal-doped ZnO films. *Materials Science and Engineering R* 2008; **62**:1-35.

[21]. Vallet-Regí M. ordered mesoporous materials in the context of drug delivery systems and bone tissue engineering. *Chem Eur J* 2006; **12**:5934-5943.

[22]. Lee J, Orilall MC, Warren SC, Kamperman M, Disalvo FJ, Wiesner U. Direct access to thermally stable and highly crystalline mesoporous transition-metal oxides with uniform pores. *Nature Materials* 2008; **7**:222-228.

[23]. Barteau MA. Organic reactions at well defined oxide surfaces. *Chem Rev* 1996; **96**:1413-1430.

[24]. Baños C, Wiedmer SK, Smått J-H, Sakeye M, Lokajová J, Riekkola M. Phospholipids covalently attached to silica particles as stationary phase in nano-liquid chromatography. *J Pharm Biomed Anal* 2012; **71**:1-10.

[25]. Smått J-H, Sayler FM, Grano AJ, Bakker MG. Formation of hierarchically porous metal oxide and metal monoliths by nanocasting into silica monoliths. *Advanced Engineering Materials* 2012; **14**:1059-1073.

[26]. Smått J-H, Spliethoff B, Rosenholm JB, Lindén M. Hierachically porous nanocrystalline cobalt oxide monoliths through nanocasting. *Chem Commun* 2004; **19**:2188-2189.

[27]. Smått J-H,Weidenthaler C, Rosenholm JB, Lindén M. Hierarchically porous metal oxide monoliths prepared by the nanocasting route. *Chem Mater* 2006; **18**:1443-1450.

[28]. Tiemann M. Repeated templating. *Chem Mater* 2008; **20**:961-971.

[29]. Gaslain FO, Parmentier J, Valtchev VP, Patarin J. First zeolite carbon replica with a well resolved X-ray diffraction pattern. *Chem Commun* 2006;991-993.

[30]. Martins CR. Membrane-based synthesis of nanomaterials. *Chem Mater* 1996; **8**:1739-1746.

[31]. Pérez-Juste J, Pastoriza-Santos I, Liz-Marzán LM, Mulvaney P. Gold nanorods: synthesis, characterization and applications. *Coord Chem Rev* 2005; **249**:1870-1901.

[32]. Stein A, Li F, Denny NR. Morphological control in colloidal crystal templating of inverse opals, hierachical structures, and shaped particles. *Chem Mater* 2008; **20**:649-666.

[33]. Stein A, Rudisill SG, Petkovich ND. Perspective on the influence of interactions between Hard and Soft Templates and precusrors on morphology of hierarchically structured porous materials. *Chem Mater* 2013; **26**:259-276.

[34]. Smått J-H. Hierarchically porous silica, carbon and metal oxide monoliths – synthesis and characterization. *Doctoral Thesis, Department of Physical Chemistry, Åbo Akademi University,* 2006.

[35]. Tüysüz H, Lehmann CW, Bongard H, Tesche B, Schmidt R, Schüth F. Direct imaging of surface topology and pore system of ordered mesoporous silica (MCM-41, SBA-15 and KIT-6) and nanocast metal oxides by high resolution scanning electron microscopy. *J AM CHEM SOC* 2008; **130**:11510-11517.

[36]. Tian B, Liu X, Yang H, Xie S, Yu C, Tu B, et al. General synthesis of ordered crystallised metal oxide nanoarrays replicated by microwave-digested mesoporous silica. *Adv Mater* 2003; **15**:1370-1374.

[37]. Haffer S, Waitz T, Tiemann M. Mesoporous In_2O_3 with regular morphology by nanocasting: a simple relation between defined particle shape and growth mechanism. *J Phys Chem C* 2010; **114**:2075-2081.

[38]. Yue W, Zhou W. Crystalline mesoporous metal oxide. *Progress in Natural Science* 2008; **18**:1329-1338.

[39]. Wang Y, Yang C-M, Schmidt W, Spliethoff B, Bill E, Schüth F, et al. Weakly ferromagnetic ordered mesoporous Co_3O_4 synthesized by nanocasting from Vinyl-functionalized Cubic *Ia3d* Mesoporous Silica. *Adv Mater* 2005; **17**:53-56.

[40]. Choi M, Heo W, Kleitz F, Ryoo R. Facile synthesis of high quality mesoporous SBA-15 with enhanced control of the porous network connectivity and wall thickness. *Chem Commun* 2003; 1340-1341.

[41]. Zhao D, Sun J, Li Q, Stucky GD. Morphological control of highly ordered mesoporous silica SBA-15. *Chem Mater* 2000; **12**:275-279.

[42]. Wan Y, Zhao D. On the controllable soft-templating approach to mesoporous silicates. *Chemical Reviews* 2007; **107**:2821-2860.

[43]. Galarneau A, Cambon H, Di Renzo F, Fajula F. True microporosity and surface area of mesoporous SBA-15 silicas as a function of synthesis temperature. *Langmuir* 2001; **17**:8328-8335.

[44]. Galarneau A, Cambon H, Di Renzo F, Ryoo R, Choib M, Fajula F. Microporosity and connections between pores in SBA-15 mesostructured silicas as a function of the temperature of synthesis. *New J Chem* 2003; **27**:73-79.

[45]. Kruk M, Jaroniec M, Ko CH, Ryoo R. Characterization of the porous structure of SBA-15. *Chem Mater* 2000; **12**:1961-1968.

[46]. Ryoo R, Ko CH, Kruk M, Antochshuk V, Jaroniec M. Block-copolymer-templated ordered mesoporous silica: array of uniform mesopores or mesopore-micropore network. *J Phys Chem B* 2000; **104**:11465-11471.

[47]. Liu Z, Terasaki O, Oshuna T, Hiraga K, Shin HJ, Ryoo R. An HREM study of channel structures in mesoporous silica SBA-15 and platinum wires produced in the channels. *CHEMPHYSCHEM* 2001; **4**:229-231.

[48]. Jun S, Joo SH, Ryoo R, Kruk M, Jaroniec M, Liu Z, et al. Synthesis of new, nanoporous carbon with hexagonally ordered mesostructure. *J Am Chem Soc* 2000; **122**:10712-10713.

[49]. Sculley JP, Zhou H. Enhancing amine-supported materials for ambient air capture. *Angew Chem Int Ed* 2012; **51**:12660-12661.

[50]. Yang H, Zhao D. Synthesis of replica mesostructures by the nanocasting strategy. *J Mater Chem* 2005; **15**:1217-1231.

[51]. Dickinson C, Zhou WZ, Hodgkins RP, Yifeng, Dongyuan, Heyong. Formation mechanism of porous single crystal Cr_2O_3 and Co_3O_4 templated by mesoporous silica. *Chem Mater* 2006; **18**:3088-3095.

[52]. Wang YM, Wu ZY, Wang HJ, Zhu JH. Fabrication of metal oxides occluded in ordered mesoporoushosts via a solid-state grinding route: Influence of host-guest interactions. *Adv Funct Mater* 2006; **16**:2374-2386.

[53]. Yue W, Zhou W. Synthesis of porous single crystals of metal oxides via a solid-liquid route. *Chem Mater* 2007; **19**:2359-2363.

[54]. Wan Y, Yang H, Zhao D. "Host-Guest" chemistry in the synthesis of ordered non-siliceous mesoporous materials. *Accounts of Chemical research* 2006; **39**:423-432.

[55]. van der Meer J, Bardez-Giboire I, Mercier C, Revel B, Davidson A, Denoyel R. Mechanism of metal oxide nanoparticle loading in SBA-15 by the double solvent technique. *J Phys Chem C* 2010; **114**:3507-3515.

[56]. Burkett SL, Sims SD, Mann S. Synthesis of hybrid inorganic–organic mesoporous silica by co-condensation of siloxane and organosiloxane precursors. *Chem Commun* 1996;1367-1368.

[57]. Liu H, Du X, Xing X, Wang G, Qiao SZ. Highly ordered mesoporous Cr_2O_3 materials with enhanced performance for gas sensors and lithium ion batteries. *Chem Commun* 2012; **48**:865-867.

[58]. Tian B, Liu X, Solovyov LA, Liu Z, Yang H, Zhang Z, et al. Facile Synthesis and Characterization of Novel Mesoporous and Mesorelief Oxides with Gyroidal Structures. *J Am Chem Soc* 2004; **126**:865-875.

[59]. Sun X, Shi Y, Zhang P, Zheng C, Zheng X, Zhang F, et al. Container Effect in Nanocasting Synthesis of Mesoporous Metal Oxides. *J Am Chem Soc* 2011; **133**:14542-14545.

[60]. Regonini D, Jaroenworaluck A, Stevensa R, Bowen CR. Effect of heat treatment on the properties and structure of TiO2 nanotubes: phase composition and chemical composition. *Surf Interface Anal* 2010; **42**:139-144.

[61]. Korotcenkov G. Gas response control through structural and chemical modification of metal oxide films: state of the art and approaches. *Sens Actuators B* 2005; **107**:209-232.

[62]. Hanaor DAH, Sorrell CC. Review of the anatase to rutile phase transormation. *J Mater Sci* 2011; **46**:855-874.

[63]. Kurganov A, Kuzmenko O, Davankov VA, Eray B, Unger KK, Trüdinger U. Effect of polystyrene coating on pore, structural and chromatographic properties of silica packings. *J Chromatogr A* 1990; **506**:391-400.

[64]. Hanson M, Kurganov A, Unger KK, Davankov VA. Polymer-coated reversed-phase packings in high-performance liquid chromatography. *J Chromatogr A* 1993; **656**:369-380.

[65]. Blackwell JA, Carr PW. Fluoride-modified zirconium oxide as a biocompatible stationary phase for high-performance liquid chromatography. *J Chromatogr A* 1991; **549**:59-75.

[66]. Leitner A. Phosphopeptide enrichment using metal oxide affinity chromatography. *Trends in Analytical Chemistry* 2010; **29**:177-185.

[67]. Adden N, Gamble L, Castner D, Hoffmann A, Gross G, Menzel H. Phosphonic acid monolayers for binding of bioactive molecules to titanium surfaces. *Langmuir* 2006; **22**:8197-8204.

[68]. Nawrocki J, Rigney M, McCormick A, Carr PW. Chemistry of zirconia and its use in chromatography. *J Chromatogr A* 1993; **657**:229-282.

[69]. Salazar-Alvarez G, Ahniyaz A, Villaluenga I, Berriozalab G, De Miguel YR, Bergstrom L. Dispersion and surface functionalization of oxide nanoparticles for transparent photocatalytic and UV-protecting coatings and sunscreens. *Sci Technol Adv Mater* 2013; **14**:1-23.

[70]. Marcinko S, Fadeev AY. Hydrolytic stability of organic monolayers supported on TiO_2 and ZrO_2. *Langmuir* 2004; **20**:2270-2273.

[71]. Hoogeveen NG, Stuart MAC, Fleer GJ. Polyelectrolyte adsorption on oxides: I. Kinetics and adsorbed amounts. *J Colloid Interface Sci* 1996; **182**:133-145.

[72]. Wu C, Tzeng L, Kuo Y, Shu CH. Enhancement of the photocatalytic activity of TiO_2 film via surface modification of the substrate. *Applied Catalysis A: General* 2002; **226**:199-211.

[73]. Schüth F, Sing KSW, Weitkamp J. *Handbook of Porous Solids*. 2002; **3**.

[74]. Takeuchi T. Capillary columns in liquid chromatography. *Anal Bioanal Chem* 2003; **375**:26-27.

[75]. Buchmeiser MR. New synthetic ways for the preparation of high-performance liquid chromatography supports. *J Chromatogr A* 2001; **918**:233-266.

[76]. Namera A, Nakamoto A, Saito T, Miyazaki S. Monolith as a new sample preparation material: Recent devices and applications. *J Sep Sci* 2011; **34**:901-924.

[77]. Ohkubo A, Kanda T, Ohtsu Y, Yamaguchi M. Synthesis and characterization of a strong cation exchanger based on polymer-coated silica for high-performance liquid chromatography. *J Chromatogr. A* 1997; **779**:113-122.

[78]. Pyell U. Advances in column technology and instrumentation in capillary electrochromatography. *J Chromatogr A* 2000; **892**:257-278.

[79]. Mercier J-, Morin P, Dreux M, Tambute A. Capillary electrophoresis separation of alkylphosphonic acid monoesters with indirect ultraviolet detection. *J Chromatogr A* 1997; **779**:245-252.

[80]. Shi Z-G, Feng Y-Q, Xu L, Zhang M, Da S-L. Preparation and evaluation of zirconia-coated silica monolith for capillary electrochromatography. *Talanta* 2004; **63**:593-598.

[81]. Dittmann MM, Rozing GP. Capillary electrochromatography — a high-efficiency micro-separation technique. *J Chromatogr A* 1996; **744**:63-74.

[82]. Bartle KD, Myers P. Theory of capillary electrochromatography. *J Chromatogr A* 2001; **916**:3-23.

[83]. Leitner A, Sturm M, Lindner W. Tools for analyzing the phosphoproteome and other phosphorylated biomolecules: A review. *Anal Chim Acta* 2011; **703**:19-30.

[84]. Dunn JD, Reid GE, Bruening ML. Techniques for phosphopeptide enrichment prior to analysis by mass spectrometry. *Mass Spectrom Rev* 2010; **29**:29-54.

[85]. Wang Y, Chen W, Wu J, Guo Y, Xia X. Highly efficient and selective enrichment of phosphopeptides using porous anodic alumina membrane for MALDI-TOF MS analysis. *J Am Soc Mass Spectrom* 2007; **18**:1387-1395.

[86]. Han L, Shan Z, Chen D, Yu X, Yang P, Tu B, et al. Mesoporous Fe2O3 microspheres: Rapid and effective enrichment of phosphopeptides for MALDI-TOF MS analysis. *J Colloid Interface Sci* 2008; **318**:315-321.

[87]. Li Y, Lin H, Deng C, Yang P, Zhang X. Highly selective and rapid enrichment of phosphorylated peptides using gallium oxide-coated magnetic microspheres for MALDI-TOF-MS and nano-LC-ESI-MS/MS/MS analysis. *Proteomics* 2008; **8**:238-249.

[88]. Leitner A, Sturm M, Hudecz O, Mazanek M, Smått J-, Lindén M, et al. Probing the phosphoproteome of HeLa cells using nanocast metal oxide microspheres for phosphopeptide enrichment. *Anal Chem* 2010; **82**:2726-2733.

[89]. Li X, Chen X, Sun H, Yuan B, Feng Y. Perovskite for the highly selective enrichment of phosphopeptides. *J Chromatogr A* 2015; **1376**:143-148.

[90]. Myller A, Karhe J, Pakkanen T. Preparation of Amino-functionalized TiO_2 Surfaces by Binding of Organophosphates. *Appl Surf Sci* 2010; **257**:1616-1622.

[91]. Rosenholm JM, Lindén M. Wet chemical analysis of surface concentration of accessible groups on diffrent amino-functionlaised mesporpous SBA-15 silicas. *Chem Mater* 2007; **19**:5023-5034.

[92]. McCaldin D. The chemistry of nyhindrin. *Chem Rev* 1960; **60**:39-51.

[93]. Glatter O, Kratky O. Small Angle X – ray Scattering. *London: Academic Press*; 1982.

[94]. Lind A. Characterization and hierarchical ordering of surfactant templated mesoporous silica synthesized under alkaline conditions. *Doctoral Thesis, Department of Physical Chemistry, Åbo Akademi University,* 2003.

[95]. Hunter RJ. Zeta potential in colloid science. *London: Academic Press*; 1988.

[96]. Brookhaven Instruments Corporation. *Brookhaven zeta potential analyzers user manual.* Brookhaven Instruments Corporation; 2013.

[97]. Lowell S, Shields JE, Thomas MA, Thommes M. Characterization of porous solids and powders: surface area, pore size and density. *London: Kluwer Academic Publishers*; 2004.

[98]. Atkins P, De Paula J. Elements of physical chemistry. *Oxford U P* 2009; **5**.

[99]. Neimark AV, Ravikovitch PI. Capillary condensation in MMS and pore structure characterization. *Microporous and Mesoporous Materials* 2001; **44–45**:697-707.

[100]. Ravikovitch PI, Haller GL, Neimark AV. Density functional theory model for calculating pore size distributions: pore structure of nanoporous catalysts. *Adv Colloid Interface Sci* 1998; **76–77**:203-226.

[101]. FEI C. An Introduction to Electron Microscopy. *http://www.nanolab.ucla.edu/ /pdf/* culled on 1.09.2015.

[102]. Järn M. Influence of topography and surface chemistry on the wetting properties of TiO_2-based ceramic coatings. *Laboratory of Physical Chemistry, Åbo Akademi University, Åbo, Finland* 2010.

[103]. Keely WM, Maynor HW. Thermal Studies of Nickel, Cobalt,Iron and Copper Oxides and Nitrates. *Journal of Chemical and Engineering Data* 1963; **8**:297-300.

[104]. Bach S, Henry M, Baffier N, Livage J. Sol-gel synthesis of manganese oxides. *Journal of Solid State Chemistry* 1990; **88**:325-333.

[105]. Sugiyama SN, Masuda T, Shinoda K, Nakamura A, Tomita M, Ishihama Y. Phosphopeptide enrichment by aliphatic hydroxy acid-modified metal oxide chromatography for Nano-LC-MS/MS in Proteomics Applications. *Mol Cell Preteomics* 2007; **6**:1103-1109.

[106]. Jeong NC, Lee JS, Tae EL, Lee YJ, Yoon KB. Acidity scale for metal oxides and Sanderson's electronegativities of lanthanide elements. *Angew Chem Int Ed* 2008; **47**:10128-10132.

ISBN 978-952-12-3376-0